R-08-28

Experimental studies on the interactions between anaerobically corroding iron and bentonite

Liisa Carlson, Geological Survey of Finland

Ola Karnland, Siv Olsson, Clay Technology AB

Andy Rance, Nick Smart, Serco Assurance

June 2008

Svensk Kärnbränslehantering AB
Swedish Nuclear Fuel
and Waste Management Co
Box 250, SE-101 24 Stockholm
Tel +46 8 459 84 00

SKB

ISSN 1402-3091
SKB Rapport R-08-28

Experimental studies on the interactions between anaerobically corroding iron and bentonite

Liisa Carlson, Geological Survey of Finland

Ola Karnland, Siv Olsson, Clay Technology AB

Andy Rance, Nick Smart, Serco Assurance

June 2008

Keywords: Bentonite, Iron, Corrosion, Anaerobic, Cation exchange capacity, Swelling pressure, Hydraulic conductivity.

This report is a result of a joint project between SKB and Posiva. This report is also printed as a Posiva WR report, Posiva WR 2006-60.

A pdf version of this document can be downloaded from www.skb.se.

Abstract

Anaerobic corrosion experiments using compacted bentonite, carbon steel and cast iron coupons, and carbon steel wires, were performed at temperatures of 30°C and 50°C. Dry Wyoming bentonite MX-80 powder was mixed with pieces of wire, and then compacted in stainless steel holders. The samples were evacuated and placed in test cells under nitrogen. For the coupon tests, the coupons were placed in the upper and lower part of cells filled with compacted bentonite. The compacted bentonite samples were immersed in deaerated artificial ground water containing sodium chloride and sodium carbonate at pH 10.4. The experiments with coupons ran for 356 days at 50°C and for 900 days at 30°C and the experiments with wires ran for 829 days at 30°C and for 911 days at 50°C.

Corrosion products on the surface of wires and coupons were examined using Raman spectroscopy, scanning electron microscopy and electron microprobe analysis. A mixture of magnetite, hematite and goethite was found on the surface of coupons. Only magnetite was observed on the surface of wires. The bentonite was examined using X-ray diffraction (XRD), scanning electron microscopy (SEM), electron microprobe analysis (EPMA), Raman spectroscopy, Mössbauer transmission spectroscopy, Fourier transform infrared spectroscopy (FTIR) and transmission electron microscopy (TEM) with energy dispersive spectroscopy (EDS) and selected area electron diffraction. In addition, cation exchange capacity and exchangeable cations as well as total chemical composition were determined. Hydraulic conductivity and swelling pressure were also measured.

In the coupon tests, increased iron contents could be observed in a thin contact zone. Sodium from the synthetic ground water had substituted for a fraction of the calcium in the interlayer positions of montmorillonite, which could be seen also in the total contents of these elements. A small increase in hydraulic conductivity was observed.

In the wire tests a high iron/bentonite ratio was used. Therefore, the total iron content of the bentonite increased by 6–8 percentage units and the colour turned greenish black. Cation exchange capacity of the bentonite was reduced and hydraulic conductivity increased. The proportion of iron in the Fe^{2+} oxidation state increased from 36% in fresh bentonite to 74–78%. Some of the Fe^{3+} in the octahedral montmorillonite sheets may have been reduced to Fe^{2+}. No Fe-rich clay minerals were formed. No iron oxyhydroxide minerals such as magnetite or $Fe(OH)_2$ could be identified with the methods used. Mössbauer analysis indicated the presence of adsorbed or absorbed Fe(II) but the presence of a green rust could not be ruled out. The increase in iron content of the wire bentonites probably has several explanations, including surface adsorption and substitution of some Na^+ in the interlayer positions of montmorillonite by non-exchangeable Fe(II) complexes There may also have been some very unstable oxidised iron compound present that could not be identified.

Contents

1 Introduction

Anaerobic corrosion experiments using compacted bentonite and carbon steel and cast iron coupons, and carbon steel wires, at temperatures of 30°C and 50°C were performed at Serco Assurance's laboratory at Culham, Oxfordshire. The experimental design is described in detail by /Smart et al. 2004/. The experiments were used to measure the amount of hydrogen generated by the anaerobic corrosion of steel in compacted bentonite. Two gas cells were set up with carbon steel wires embedded in compacted MX-80 bentonite clay, at two test temperatures (30°C and 50°C). In addition two test cells were set up containing coupons of cast iron and carbon steel embedded in compacted bentonite.

For the tests with wires, 5 mm lengths of 0.4 mm diameter carbon steel wire were used (BS4360 grade 43A EN 10248-1, composition, wt%: C 0.21; Si 0.220; Mn 0.7; S 0.017; P 0.017, Fe bal.). Approximately 15,300 wires were added to the test cell, giving a total surface area of about 0.1 m^2, a volume of about 9.6 cm^3 and a mass of around 75 g. The iron wires were added to bentonite powder prior to compaction of the samples and the wires were fairly evenly distributed within the samples. The test cell volume was ~ 42 cm^3, of which compacted bentonite (MX-80, 2 g/cm^3) formed a volume of about 32.3 cm^3 (64.6 g). The estimated swelling pressure for this density of bentonite is approximately 7 MPa.

In the coupon tests, the carbon steel coupons (composition, wt%: C 0.035; Si 0.011; Mn 0.18; S 0.012; P 0.011, Fe bal.) were 1 mm thick and the cast iron coupons (composition, wt%: C 3.65; Si 2.29; Mn 0.26; S < 0.005; P < 0.005, Fe bal.) were 3 mm thick. The coupons were sectors (1/6ths) cut from rings of outside diameter 38 mm and inside diameter 10 mm. One carbon steel test coupon was placed in the upper part of the cell and the other cast iron coupon was located close to the bottom. The total surface area of the carbon steel and cast iron coupons was 0.0009 m^2, with a mass of 5.5 g. In this case about 1.7% of the cell volume was made up of iron.

To minimise the amount of surface oxide present at the start of the experiments, the metal specimens were pickled in hydrochloric acid and then thoroughly rinsed in deionised water. After pickling, the specimens were stored under nitrogen until they were mixed with powdered MX-80 bentonite clay, a sodium montmorillonite, in specially designed stainless steel sample holders that allowed penetration of artificial groundwater into the bentonite when it was wetted, but restricted the expansion of the bentonite and generated a swelling pressure.

After setting up the test specimens in the compacted bentonite holders they were evacuated and then transferred into a nitrogen-purged glove box where they were placed in the gas cells and immersed in a simple, deaerated artificial groundwater containing 31.56 g/litre sodium chloride and 1.06 g/litre sodium carbonate, with an 'as prepared' pH of ~ 10.4. The samples were then sealed in the gas cells, removed from the glove box (N_2 < 10 ppm) and monitored for several months. This report describes the analyses that were carried out when the four tests were dismantled after the corrosion experiments were completed.

2 Objectives

The purpose of this project was to investigate how the mineralogical, chemical and technical characteristics of bentonite are changed by contact with carbon steel/cast iron in anoxic conditions and to identify what kind of corrosion products are formed in the contact zone between corroding metal and bentonite.

Possible changes that might be expected in bentonite as a result of contact with corroding steel are as follows:

1) Ferrous iron substitutes for Na^+ in the interlayer position of montmorillonite This has been observed in several tests, for example by /Kamei et al. 1999/ and /Idemitsu et al. 2003/.
2) Fe-compounds are formed, e.g. magnetite and/or $Fe(OH)_2$. Several theoretical calculations predict their formation /e.g. Xia et al. 2004/.
3) The presence of metallic iron could bring about reduction of octahedral Fe^{3+} in montmorillonite. Reduction has been reported from tests performed in the presence of iron-reducing bacteria /Kostka et al. 1999/ and strong reducers like Na-dithionite /Stucki et al. 1984/.
4) Transformation of montmorillonite to an Fe-rich phase like berthierine ($Fe^{2+}_{1.5}AlFe^{3+}_{0.2}Mg_{0.2}Si_{1.1}Al_{0.9}O_5(OH)_2$) or chlorite [$(Fe,Mg,Al)_6(Si,Al)_4O_{10}(OH)_8$]. Formation of a 7 Å phase (berthierine-cronstedtite-odinite) at 80°C was reported by /Lantenois 2003/ in experiments where bentonite was kept in contact with powdered metallic iron. According to /Wilson et al. 2005/ significant alteration to Fe-rich smectite and a 7 Å phase was observed at 250°C but not at 80°C or 150°C. Formation of a high-charge Fe^{2+}-rich smectite (saponite-like) and chlorite has been reported at a temperature of 300°C /Guillaume et al. 2003/.

Changes in the octahedral montmorillonite sheets (i.e. (3) above) change the charge distribution in the interlayers and this might affect many technologically important properties of bentonites, for example cation exchange capacity, swelling pressure and hydraulic conductivity. Reduction of octahedral iron leads to an increase in layer charge that should bring about an increase in cation exchange capacity. However, /Lear and Stucki 1989/ found a significant inverse correlation between specific surface area and Fe^{2+} content in nontronite. Reduction of Fe^{3+} could lead to collapse of expanded layers and Na-fixation and, consequently, to a decrease in cation exchange capacity. Progressive loss of OH groups from octahedral sheets of nontronite as a function of duration of reduction was observed by /Fialips et al. 2002/. Furthermore, the transformation of montmorillonite into Fe-rich phases like berthierine or chlorite (i.e. (4) above) strongly affects the physicochemical properties of bentonite, but these phases are only expected to form at temperatures higher than those applied in the present study.

Serco Assurance was responsible for the following determinations: Scanning electron microscopy with energy dispersive X-ray detector and electron microprobe analysis (SEM-EDX and EPMA), Laser Raman spectroscopy, anoxic X-ray powder diffraction (XRD) and Mössbauer spectroscopy. Geological Survey of Finland (GSF) was responsible for the completion of oxic XRD, Fourier transform infrared spectroscopy (FTIR), transmission electron microscopy with energy dispersive spectrometry (TEM-EDS), the determination of cation exchange capacity (CEC) and exchangeable cations as well as the determination of total chemical composition. Clay Technology was responsible for the determinations of swelling pressure and hydraulic conductivity and for some additional determinations of CEC.

3 Description of samples

The visual appearance and texture of the corrosion samples are presented in Appendix 1. Samples from two of the four corrosion tests were studied in the first stage, one with cast iron and carbon steel coupons (356 days exposure at 50°C, the 'coupon 50C sample/bentonite'), and one with carbon steel wires (829 days exposure at 30°C, the 'wire 30C sample/bentonite'). In the second stage, samples from the remaining two tests were studied, again one with cast iron and carbon steel coupons (900 days at 30°C, the 'coupon 30C sample/bentonite') and one with carbon steel wires (911 days at 50°C, the 'wire 50C sample/bentonite'). After dismantling the cells, the samples were kept in a nitrogen-purged glove box where the samples were prepared for analysis. The cast iron and carbon steel coupons were removed and analysed and the residual compacted bentonite was used to develop techniques for cutting the material and separating the bentonite from the corroded steel. When the compacted bentonite sample containing carbon steel wire was removed from the sample holder, it was found to be quite crumbly and it disintegrated when attempts were made to cut slices from it. The bentonite was sliced into 5 to 10 mm lengths and the slices were ground gently in a pestle and mortar to break them apart.

The coupon samples looked like typical compacted bentonite (i.e. predominantly grey). Black and brownish precipitate could be seen in the contact zone from where the coupon had been removed. The wire 30 sample was a mixture of wire pieces with greenish-black bentonite. The pieces of carbon steel wire were removed from the bentonite in the wire 50C sample by separation by hand. Two reference samples were studied in parallel to the corrosion samples – these were MX-80, which is the bentonite that was used for the corrosion experiments, and Kutch 8939, which is an Fe-rich bentonite from India (for details, see /Carlson 2004/; the producer Ashapura Minechem Limited now uses the name Asha 505).

For transporting the first set of samples for analysis (e.g. to GSF), subsamples of a few grams each were sealed in separate plastic bags that were then placed in glass vessels with a screw cap. The glass vessels were then sealed into two further plastic bags, to provide in total three plastic barriers and the glass vessel. All this packaging was carried out in the inert nitrogen atmosphere in the glovebox. The plastic bags were sealed using a thermal plastic welder. Tests using oxygen sensitive indicator liquid showed that this procedure was effective in sealing the samples from contact with the air. The second set of subsamples was sealed in separate plastic bags that were sealed into two further plastic bags using a thermal plastic welder.

4 Analytical METHODS

4.1 XRD (oxic)

4.1.1 Oriented mounts of clay fraction

Oriented mounts of the first set of samples were prepared for X-ray powder diffraction. In such mounts the platy clay mineral particles lie parallel to the surface of the preparation and the characteristic basal reflections are enhanced. The preparation was carried out in a nitrogen-purged glove box (for details, see 4.7). The coupon 50C bentonite was ground in an agate mortar after removing the brownish black contact zone and mixed in a centrifuge tube with MilliQ water that was purged with instrument N_2 in the glove box. The wire 30C bentonite that contained pieces of wire was suspended in the N_2-purged MilliQ water and the suspension without wires was decanted to a centrifuge tube in the glove box. Both samples were allowed to swell for 4 hours, after which the centrifuge tubes were closed with airtight stoppers, removed from the glove box and centrifuged for 10 minutes at 4,000G max. The centrifuge tubes were then brought back to the glove box and the water was decanted. The gel-like swollen bentonite from the top layer was spread on glass slides, which were allowed to dry in the glove box overnight. Preparation of an oriented mount of MX-80 was performed in air in a similar manner by swelling for four hours, centrifuging, spreading the top layer on glass slides and drying in air. The prepared samples were brought to the XRD laboratory within one hour of removal from the glove box and the first scans from 2 to 20°2Θ were obtained immediately (20 minutes per sample). For comparison, MX-80 was run after the scans on the material from the corrosion tests. Additional XRD scans over the range 2 to 70°2Θ were performed within 2 to 3 hours and subsequently MX-80 was run again.

The XRD data was collected on a Philips X'Pert diffractometer equipped with a vertical goniometer, a diffracted beam monochromator, progressive divergence and receiving slits and a rotating sample holder at the Research Laboratory of the Geological Survey of Finland. Cu Kα-radiation was used and the applied voltage was 40 kV with a 55 mA current. The counting time was 1 s per 0.02°2Θ.

The position of the (001) basal peak of montmorillonite is sensitive to relative humidity and type of interlayer cations. Because the relative humidity of the glove box was very low (not measured), the preparations were allowed to equilibrate with the relative humidity of the laboratory. Relative humidity affects the number of water layers in the interlayer position of montmorillonite and thus the d-spacings of all basal reflections. In order to be able to compare the positions of the (001) peaks in bentonite from the corrosion tests it would be necessary to ensure that the humidity was the same for all samples prepared for XRD analysis.

The colour of the bentonite preparations from the corrosion tests differed from that of fresh MX-80. The coupon sample was somewhat lighter grey and the wire sample was green (Figure 4-1). The green colour did not change in air, showing that apparently no oxidation occurred in the dry state. A non-oriented mount of the wire 30C sample was prepared from a bentonite-wire-water mixture left over from a preparation for FTIR measurements.

The bentonite slurry was spread on a glass slide and allowed to dry in air at room temperature. Because pieces of wire had not been removed from the sample it is probable that corrosion continued as long as the mixture was wet. One more mount was prepared of a wet wire-sample that was kept in the glove box after preparation of the oriented mount. The slurry, which was still greenish-black, was smeared on a glass slide and dried overnight at room temperature. The colour turned brown on oxidation.

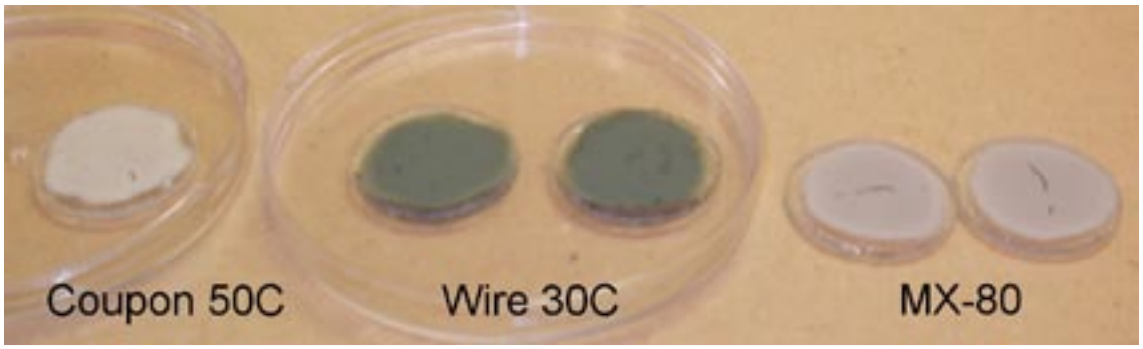

Figure 4-1. *Oriented mounts for XRD analysis, prepared in a N_2-filled glove box.*

4.1.2 Random mounts of bulk samples

Because of problems with relative humidity control for oriented mounts prepared in the glove box and with oxidation of iron when the wire sample was wetted in air, preparation of the second set of samples (coupon 30C and wire 50C), as well as the control samples MX-80 and Kutch 8939, was performed dry. The samples were ground in an agate mortar and the powder was pressed in a sample holder. Pressing caused partial orientation of platy grains/aggregates. The brownish black contact zone in the specimen from the coupon 30C bentonite test was removed before powdering the sample. The diffractograms were recorded over the range 2 to 70°2Θ as described above. The relative humidity of the laboratory was 45–50% during preparation and XRD scans of the second set of samples.

4.2 XRD anoxic

XRD patterns for the air-sensitive corrosion samples were obtained on powders by sealing them under nitrogen in glass X-ray tubes. No steps were taken to orientate the crystals in the samples. A reference MX-80 sample was prepared for XRD analysis in a similar manner in the glove box. Both coupon samples powdered for XRD contained the brownish black contact zone as well as grey bentonite outside the contact zone. For comparison, a preparation of the coupon 50C bentonite was obtained in air and another after the sample was wrapped in Mylar film, to determine whether Mylar could be used as a material for protecting samples from exposure to air and/or moisture.

X-ray diffraction (XRD) analysis was carried out using a fully automated Siemens D500 powder diffractometer employing CuKα radiation (wavelength 0.15406 nm) and a secondary monochromator. The samples (except those contained in glass capillaries) were continuously spun during data collection and were scanned using a step size of 0.05°2Θ in the range of 5–75°2Θ with a count time of 15 seconds per step.

4.3 Laser Raman Spectroscopy

Laser Raman spectra were obtained for the corrosion products on the two coupons as well as on corroded wires and the bentonite. The coupon samples were sealed in a plastic box fitted with an optical flat. The wires, some of which were attached to residual bentonite, were sealed under nitrogen in glass tubes using epoxy resin. After removal from the glove box, the glass itself was sealed with a blowtorch to ensure air-free conditions inside. This operation was carried out well away from the sample so that it did not experience any heating.

A Renishaw laser Raman Microscope was used to analyse the samples in situ, directly through the optical window or glass capillary. Raman spectroscopy is an optical technique whereby

chemical and phase specific information can be obtained non-destructively. Spectra were recorded in the back-scattered geometry using a ×50 high numerical aperture objective lens, giving a spatial resolution of some 4 μm. The exciting laser wavelength was 688 nm (from an air cooled He^+ ion laser). The power was approximately 100 mW. By pointing the laser beam at the point of interest it was possible to obtain spectra for bentonite and corrosion product using the same sample.

The intensity and position of the bands in a laser Raman spectrum depend both on the chemical composition and the crystal phase composition of the sample. Identification of corrosion products was achieved by comparing their spectra with those of standards.

4.4 SEM-EDX and SEM-EPMA

SEM-EDX and SEM-EPMA were used to investigate both the coupon bentonite and the mixture of wires and bentonite. The objective of the analyses was to determine the extent, if any, of iron penetration into the clay. SEM images and EDX analyses were obtained on samples that were examined as loose powder, wires or coupons using the JEOL 840a SEM and the Oxford Instruments ISIS Energy Dispersive X-ray detector. Semi-quantitative EPMA analysis was carried out on cross-sections taken through the bentonite in the contact area with the coupons or wires using a Jeol 8800 Superprobe. The cross-sections were prepared by mounting in epoxy resin and grinding, inside a nitrogen-purged glovebox. The samples were then carbon coated. The carbon coating process involved keeping the sample in vacuum for several hours, during which the samples contracted due to loss of water. Therefore, the surfaces were not as flat and smooth as required for accurate EPMA analysis. Both point analyses and elemental maps were obtained on the cross-sections. The samples were mapped for Fe, S, and Ca in the EPMA, at a number of magnifications.

4.5 Mössbauer spectroscopy

Mössbauer spectra were obtained for the material, which was prepared and stored under nitrogen until it was transferred to the Mössbauer instrument, where it was measured under liquid nitrogen. The presence of liquid nitrogen would have ensured that the samples were not exposed to air during the measurements. The Mössbauer spectra were obtained at 80K using a Wissel spectrometer. A Wissel Mössbauer drive unit MDU-1200, DFG-1000, MVC-450 and a Canberra amplifier 2012 were utilised in the data collection. A triangular wave with 1024 channels was used which was subsequently folded to 512 channels on fitting. The source was cobalt 57 in rhodium (25 mCi). The resulting spectral data sets were collected on a PC via a Wissel CMCA-550 ISA data collection card utilizing Wissoft'98 collection software. The data sets were then fitted to Lorentzian line shapes using Wissel Normos Version 9.0. Spectra are quoted relative to a 25 mm natural iron foil.

4.6 FTIR

The bentonite samples were ground in an agate mortar and the powder was used for pressing pellets for FTIR. In the case of the wire bentonites that were easily oxidized, care was taken to ensure that the samples were ground, the pellets pressed and the spectra recorded as soon as possible after removing the samples from the glove box. The colour of the powder was green. For comparison, some wire 30C bentonite was mixed with deionised water and the suspension decanted and dried at 80°C. In the top layer, the green colour turned brown indicating the formation of iron oxides. Some greenish material was left on the bottom. The sample was ground in an agate mortar and pellets were pressed for FTIR. Additional spectra were recorded of the ground wire 50C bentonite sample after 4 days in air and of the clay fraction of the wire 30C

bentonite dried in a glove box and kept for 6 weeks in air. The colour of the wire 30C bentonite sample remained unchanged in air, whereas the colour of the wire 50C bentonite gradually turned olive green, indicating some oxidation of iron. Two ratios of sample to KBr were used when preparing the samples for FTIR, namely 3 mg/200 mg KBr or 0.4 mg/200 mg KBr. The first ratio is better for the observation of OH-stretching frequencies at wavenumbers 3,000–4,000 cm^{-1} and the second is better for the observation of OH-bending frequencies at wavenumbers 800–1,000 cm^{-1}. In the OH-stretching frequencies the bands coincided so that a curve-fitting program would have been necessary to resolve the components. Therefore, most attention was paid to the OH-bending frequencies, as was done by /Wilson et al. 2005/. The infrared transmittance spectra were obtained using a Perkin Elmer Spectrum One FT-IR spectrometer at the Department of Geology, University of Helsinki. Each spectrum consisted of 10 scans at a resolution of 4 cm^{-1}.

4.7 Exchangeable cations and CEC

Most methods to determine exchangeable cations and cation exchange capacity are based on substituting the exchangeable cations with an index cation that is provided in excess in solution and determining either the concentration of cations released or the amount of index cation consumed. Based on earlier experiments, barium was selected as the index cation. Extractions with $BaCl_2$ were performed at the Department of Chemistry, University of Helsinki both in an inert atmosphere and in air; the second set of samples was extracted only in inert atmosphere. A Braun controlled-atmosphere glove box with nitrogen filling gas was used. The O_2-concentration in the glove box was < 1 ppm and the CO_2-concentration was 0 ppm during the experiments. For the 0.1 M $BaCl_2$-solutions, reagent grade $BaCl_2 \cdot 2H_2O$ (Merck 1.01719. LOT A466119) was used. The solution for the inert atmosphere conditions was prepared by dissolving 12.20730 g of $BaCl_2 \cdot 2H_2O$ in 500 ml of fresh MilliQ water that was purged with instrument N_2 (99.999%) in the glove box. The solution for experiments in a laboratory atmosphere was prepared by dissolving 12.21286 g $BaCl_2 \cdot 2H_2O$ into 500 ml of fresh MilliQ water.

The vessels or plastic bags containing subsamples of bentonite were opened in the glove box and portions of ca. 4 g were taken for the extractions. From the coupon samples the rusty contact zone was removed and sealed in a separate glass ampoule. The samples were gently ground in an agate mortar. 5 ml glass ampoules were weighed outside the glove box. Aliquots of the ground bentonites were sealed into these ampoules and weighed outside the glove box. After weighing, the ampoules were transported into the glove box.

Determinations were performed as follows:

Samples for inert atmosphere experiments:
An aliquot was taken and the bentonite poured into a polypropylene centrifuge tube together with 35.0 ml of 0.1 M $BaCl_2$-solution. The centrifuge tubes were placed in an end-over-end mixer for six days (coupon 50C, wire 30C) or five days (coupon 30C, wire 50C). After mixing, the samples were centrifuged for 10 min (4,000 G max.) outside the glove box. The total time outside the inert atmosphere was 15 min. After separation of solution and solid by centrifugation, 20 ml of the solution was filtered through a 0.2 µm membrane filter (Millipore) and taken for analysis and the pH of the rest of the solution was measured using a Ross glass/AgCl-electrode. Calibration of the electrode was carried out using Titrisol standard pH solutions.

Samples for determinations under laboratory atmosphere:
The aliquot samples taken for experiments in the laboratory atmosphere were poured into centrifuge tubes outside the glove box and $BaCl_2$-solution prepared under oxic conditions was added to the tubes. The tubes were placed in an end-over-end mixer for six days. After mixing, the solution and solid were separated and the solution samples were taken for analysis and pH measurement.

Reference samples:
The reference bentonites were MX-80 and the Indian Kutch 8939. The Kutch 8939 bentonite was ground in an agate mortar and subsequently sieved (0.15 mm mesh size). Experiments with the reference bentonites were performed simultaneously with the coupon and wire bentonites using the same procedures in both the inert and laboratory atmospheres.

Solution from the water-bentonite slurries:
The solution decanted after centrifugation (4,000 G max.) for the preparation of XRD mounts (coupon 50C and wire 30C samples) was stored in polyethylene vials in an inert atmosphere. The solution phases were sampled for chemical analysis after centrifugation (27,000 G max, 30 min) and filtration through a 0.2 µm membrane filter. Only small aliquots could be filtered, owing probably to the high resistance in filtering caused most probably by colloidal material in the solution.

Chemical analyses:
The concentrations of Al, Fe, Ca, K, Mg, Na and Ba were determined in all extracts and in the $BaCl_2$-extractant using ICP-AES. CEC was calculated as the difference between Ba-concentration in solution before and after the extractions. Na in the solution from the water-bentonite slurries was determined using ICP-AES, chloride content was measured using ion cromatography.

Use of radioactive tracer:
For comparison, CEC of coupon 30C, wire 50C and MX-80 samples was determined using a 0.0235M solution of the radioactive barium isotope Ba-133. The percentage of sorption was measured as the decrease of activity in the solution. The accuracy of the result on the 96% level of confidence was ca 8%.

Additional CEC-determinations were performed at Clay Technology using the Cu(II)-triethylenetetramine method /Meier and Kahr 1999/. The method was slightly modified to minimise problems with incomplete exchange of divalent cations /Karnland et al. 2005/. All extractions were performed in a glove box, which was slightly over-pressurized with a nitrogen/hydrogen/carbon dioxide gas mixture. The ground sample (400 mg) was dispersed in 50 ml nitrogen purged, deionised water by ultrasonic treatment. 20 ml of 15 mM Cu(II)-triethylene-tetramine solution was added to the suspension, which was left to react for 15 minutes on a vibrating table. Thereafter the Cu-saturated clay was allowed to settle. An aliquot of the supernatant was withdrawn and replaced with an equal volume of fresh reagent solution and the procedure was repeated. After centrifugation of the solutions (under laboratory atmosphere) the absorbance at 620 nm was measured using a double-beam spectrophotometer (Perkin Elmer Lambda 3) with 1 cm quartz cuvettes. CEC was calculated on the basis of the total uptake of Cu by the clay. The water content of the clay was determined for a separate sample dried at 105°C to a constant weight.

4.8 TEM-EDS

The following samples were studied using transmission electron microscopy: bulk samples of the coupon 50C, coupon 30C, wire 30C and wire 50C bentonites, as well as clay fractions of the wire 30C bentonite and the control samples MX-80 and Kutch 8939. The coupon 30C and the wire 50C bentonites were kept in the glove box until the day before they were examined. The black colour of the wire 50C bentonite was unchanged when the sample was prepared for examination in the TEM next day. The wire 30C sample was stored in air for a couple of days and the colour turned brown because of oxidation of iron. From the two coupon samples material for analysis was taken with a surgical knife just below the brownish black zone. A small amount of sample was dispersed in ethanol and ground between glass slides. Some of the slurry

was placed on a carbon-coated copper grid. The dried preparation was immediately examined with a JEOL 2010 transmission electron microscope equipped with ThermoNoran Vantage EDS analyser at the Department of Material Sciences, Tampere University of Technology. The platy clay mineral grains/aggregates settled parallel to the grid surface and could be observed 'from above' at magnifications in the range 1:5,000–1:60,000. Five to eleven particles per sample were selected, photographed and their electron diffraction patterns recorded on photographic film. Electron diffraction was used to obtain information about the crystal structure and possible aggregation of single crystals. d-values (in Å unit) were calculated using the formula $d = \lambda \cdot L/R$, where λ is the wavelength used (0.0251 Å), L the camera length (1,000 mm) and R the distance of the dots (single crystals) or rings (aggregates) from the origin on the photographic film measured in mm. EDS-analyses were performed in two to seven points of each particle and averages and standard deviations were calculated. EDS is a semi-quantitative method and it does not differentiate between Fe^{2+} and Fe^{3+} but gives the total iron content.

4.9 Total chemical composition

The corrosion bentonites were ground in an agate mortar and the control samples, MX-80 and Kutch 8939, were pulverized in a ring mill equipped with a tungsten carbide bowl. The silicon content was determined by sodium peroxide fusion, dissolution in HF-$HClO_4$ and analysis with ICP-AES. The rest of the elements were determined with ICP-AES after lithium metaborate fusion and dissolution in HF-$HClO_4$.

4.10 Swelling pressure and hydraulic conductivity

The swelling pressure and hydraulic conductivity were measured for the bentonite material coming from the four types of corrosion tests, namely bentonite with coupons at 30°C and 50°C and bentonite with wires at 30°C and 50°C. The sealing properties normally depend approximately exponentially on bentonite density, and the material from each test type was therefore measured at several sample densities in order to enhance the evaluation.

All the following preparation and measuring activity was made under anoxic conditions in a glove box, which was slightly over-pressurized with a nitrogen/hydrogen/carbon dioxide mixture. The bentonite from the corrosion tests was separated from metallic iron by just breaking loose the coupons and the wires were removed by hand. The bentonite materials were then ground to a grain size similar to that of the original MX-80 material. Known masses of test material were placed in cylindrical test cells and compacted to the standard height of 5 mm (Figure 4-2). Pistons were placed on top of each sample and force transducers were placed and fixed on top of the pistons. The diameter of the cells was 20 mm. The small dimensions of the test cell were due to the limited supply of test material.

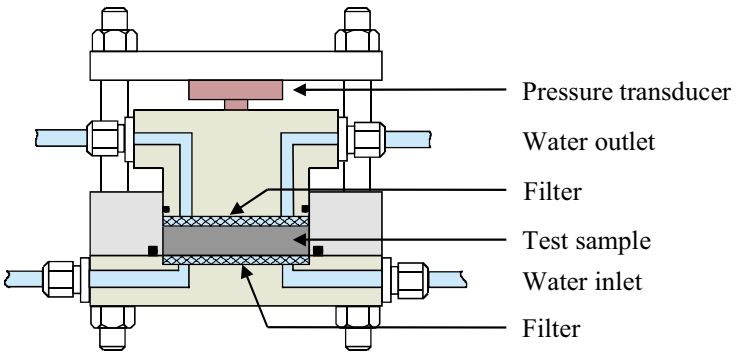

Figure 4-2. *Schematic drawing of the sample holder used in all tests.*

The samples were contacted with a nitrogen purged 0.1 M NaCl solution through filters in the upper part of the bottom lids and in the bottom part of the pistons. The swelling forces on the pistons were measured by the transducers regularly and converted into pressure by dividing by the piston area. The swelling pressure increase generally ceased after a few days and after approximately 7 days the samples were considered to be fully water saturated. The water solution pressure at the bottom side of the samples was increased to maximum of half the measured swelling pressure. The volumes of percolated solution on the upper side of the samples were measured and the hydraulic conductivities were calculated according to Darcy's law.

The solution pressure was reduced to atmospheric conditions, the samples were removed from the sample holder and the mass of each sample was determined. The samples were quickly removed from the anoxic conditions and placed in a vacuum dryer (air pressure < 0.1 kPa). After 24 h the samples were weighed and again placed in the vacuum dryer. The samples were considered dry when no further mass loss was measured. The samples were placed in a drying kiln at 105°C overnight and again weighed in order to ensure that no further water was present. The water ratio was calculated from the mass loss. The grain densities of two of the wire samples were determined by use of a pycnometer. Finally, the sample densities were calculated from the water ratio and the grain density, assuming that the water density was 1,000 kg/m^3.

5 Results

5.1 Colour of bentonite

The bentonite samples from the coupon tests was the same grey colour as fresh MX-80, except that there was a thin black zone at the contact with the coupons. During the corrosion tests with carbon steel wire the colour of the bentonite turned greenish black from the originally light grey colour. When powdered, the colour was bluish green. In air, the colour turned olive green in four days, indicating partial oxidation of iron. If wetted in air, the bentonite quickly turned brown, indicating formation of ferric oxides. Also the clay fraction of the wire 30C sample was bluish green (Figure 4-1) and it did not change in air. According to /Komadel et al. 1990/ the colour of Fe-rich smectites is indicative of the level of Fe^{2+} in the crystal structure. The green or blue-green colour occurs if Fe^{2+} and Fe^{3+} are present in adjacent sites in the octahedral sheets. If Fe is completely reduced, the colour is light grey. According to /Xia et al. 2004/, the dark-green colour is also indicative of $Fe(OH)_2$, Fe_3O_4 or their mixture.

5.2 XRD Oxic

XRD patterns of the oriented mounts of the clay fraction of MX-80, wire 30C and coupon 50C corrosion samples are presented in Figure 5-1 and Figure 5-2. The XRD profile of MX80 has a (001)-peak at ca. 12.5 Å, which is typical of the one-layer hydration state of Na-montmorillonite. However, the montmorillonite in MX80 contains also minor amounts of interlayer Ca (and Mg). The shoulder at 14.8 Å on the low angle side of the peak (Figure 5-1) is probably produced by the two-layer hydrate of Ca-montmorillonite While the one-layer Na-hydrate is stable only at relative humidities below 50–60%, the two-layer Ca-hydrate (14.8 Å) predominates over a wide range of relative humidities (ca. 25–90%; /Brindley and Brown 1980/). The variation of the d_{001} values of Fe(II)-interlayered montmorillonite with changing ambient relative humidity has been found to be in good agreement with that of divalent cations /Kamei et al. 1999, Kozai et al. 2001/. Thus, under "normal" laboratory conditions one might expect a d(001) value in the range 14–16 Å for Fe(II)-montmorillonite. Accordingly, RH values between 25 and 60% should give maximal difference between the d_{001} spacing of discrete phases of Na- and Fe(II)-montmorillonite.

In the diffraction patterns of the oriented mount of the coupon 50C corrosion sample run after 1–1.5 hours in air, the maximum intensity of the (001) peak is at 12.4 Å (Figure 5-2). After 3 days in air, a shoulder appears at 14.6 Å and the XRD-profile closely resembles that of MX-80 suggesting that Na-montmorillonite is the major component.

The maximum intensity of the (001) peak of the wire 30C corrosion sample run after 1.5 hours in air (Figure 5-1) is at 12.1 Å. However, this peak is broad and asymmetrical with a shoulder at ca.10 Å and the diffraction pattern displays an irrational series of basal reflections, with a distinct 4.85 Å peak. The pattern is indicative of an interstratified structure, which may have formed due to incorporation of iron complexes into some smectite interlayers. Alternatively, the clay was partially dehydrated when the preparations were dried in the glove box at very low relative humidity (not measured). After 3 days in air, the (001)-peak is symmetric at 12.2 Å, (Figure 5-1), possibly due to some rehydration of the clay. The XRD-profile of the sample prepared in air (uppermost curve in Figure 5-1) displays no 4.85 Å peak and the (001) peak is clearly resolved in two peaks, one at 12.7 Å, and the other at 15.2 Å. This appearance of the (001) peak can be attributed to either mixed interlayer cations, or mixed hydration states.

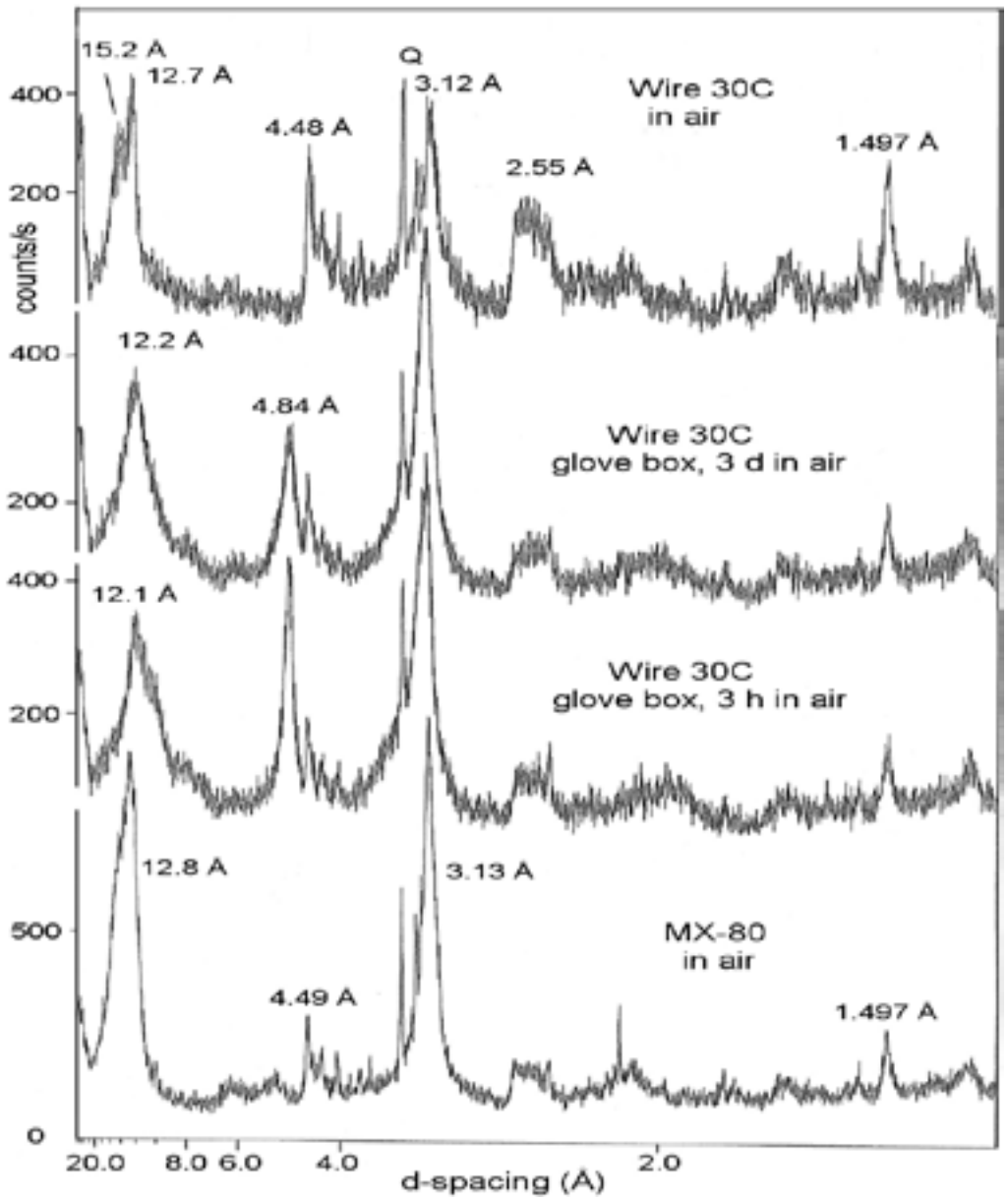

Figure 5-1. *XRD patterns of oriented mounts of wire 30C bentonite and MX-80 samples. Fractionation and preparation of sample wire 30C was carried out in a nitrogen-purged glove box and the diffractograms were recorded after 3 hours and 3 days in air, respectively. For the uppermost diffractogram the preparation was carried out in air, 2 hours after removing the wet sample from the glove box. The preparation was allowed to dry in air. The preparation of the MX-80 sample was conducted in air.*

Judged by the data on the exchangeable cations (section 5.8), a significant amount of sodium still occupies the exchange sites of the wire 30C montmorillonite, but iron in some form has substituted for some of the exchangeable cations. Hypothetically, interlayers of variable composition may have formed, giving a randomly interstratified structure. The available XRD data do not contradict such interpretation but are ambiguous. It is evident that XRD-scans have to be carried out in an inert atomsphere under controlled relative humidity in order to reliably detect these small-scale changes in smectites.

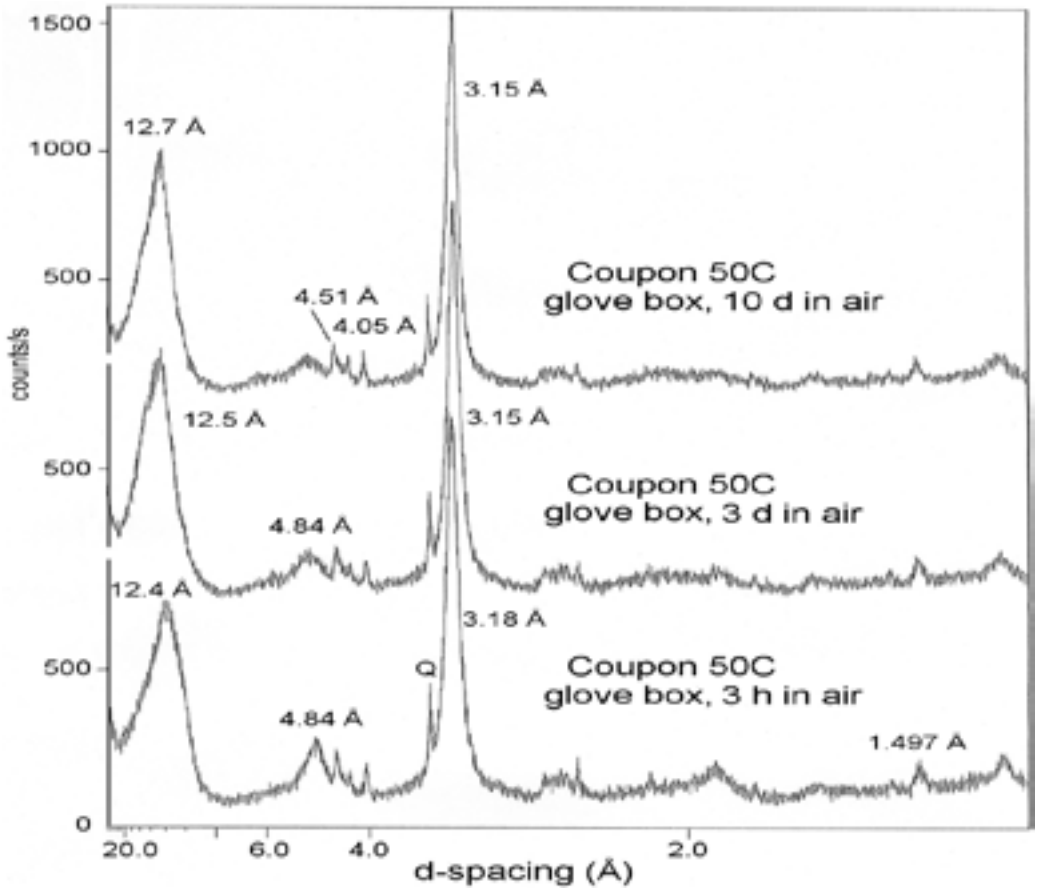

Figure 5-2. *XRD patterns of oriented mount of clay fraction of sample coupon 50C after 3 hours, 3 days and 10 days in air. The fractionation was done, the oriented mount prepared and dried in a N_2-filled glove box.*

Only random mounts were prepared of wire 50C and coupon 30C samples. The XRD patterns of the two corrosion samples as well as of the control samples MX-80 and Kutch 8939 are presented in Figure 5-3. The (001)-peak of both corrosion samples and MX-80 is at 12.4 Å. In Kutch 8939 the Ca/Na ratio in the interlayer positions is higher than in MX-80, and the (001) peak in the XRD pattern of Kutch 8939 has a more distinct shoulder on the low angle side, than MX-80. In the corrosion samples the (001) peak is symmetric at 12.4 Å, suggesting that the artificial ground water used in the corrosion tests brought about exchange of Ca for Na in the interlayer position of montmorillonite. No indication of discrete Fe-interlayered montmorillonite could be detected.

The position of the (060) peak depends on the composition of the smectite and is affected by changes in the b-parameter in the crystal lattice. The almost identical values of the (060) peak, 1.492 Å in wire 50C and 1.497 Å in MX80, indicate, that Fe had not substituted for Al or Mg in the montmorillonite octahedral sheet. Also the reduction of Fe^{3+} to Fe^{2+} in the octahedral sheets is believed to bring about an increase in the b-dimension of montmorillonite and thus also in the value of the (060)-peak /e.g.Vicente et al. 1998/. Apparently, the total iron content of the octahedral sheets is so low that a change in its oxidation state does not significantly affect the value of the (060) peak, which mainly reflects the high Al content of the octahedral sheets.

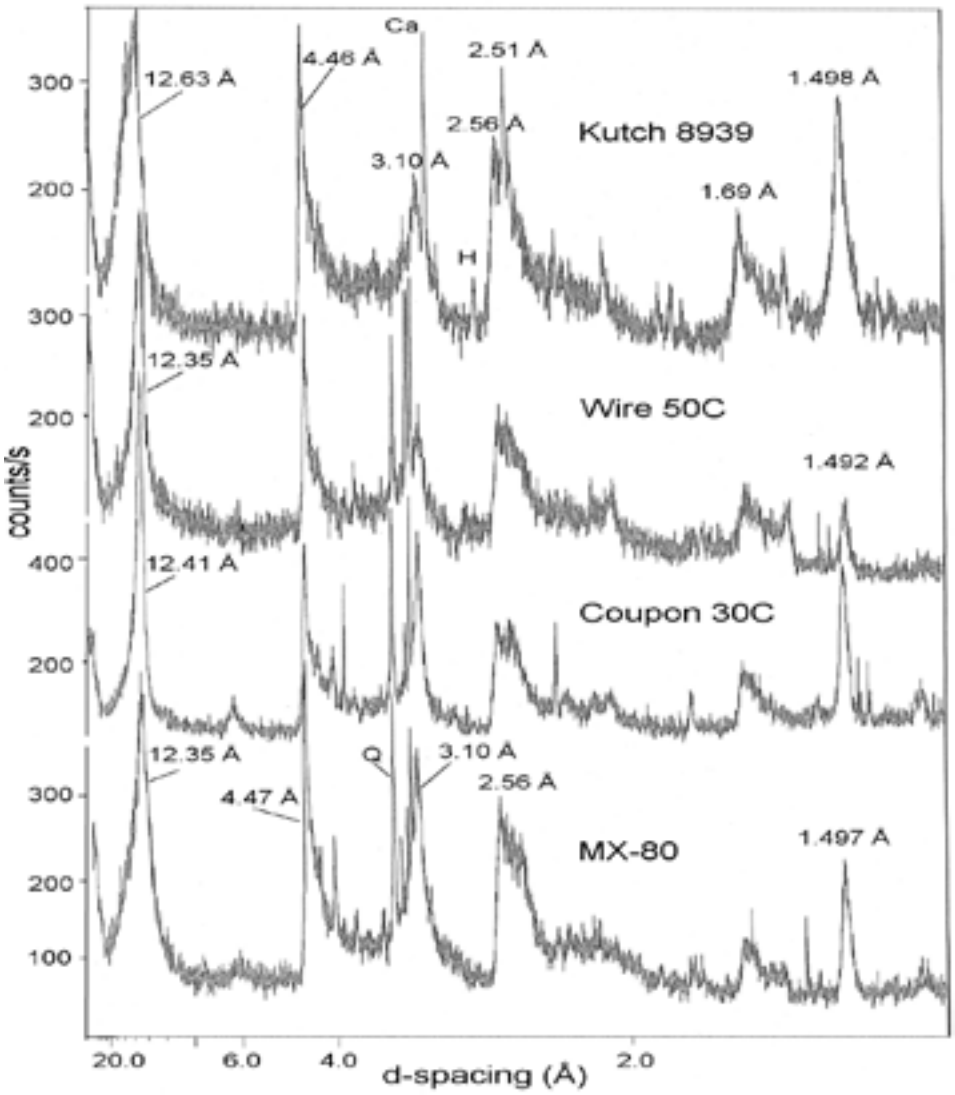

Figure 5-3. *X-ray diffractograms of random mounts. d-spacings of selected montmorillonite peaks are given. The main peaks of other minerals are labelled: Q, quartz, Ca, calcite, H, hematite/goethite.*

No well-crystallized iron oxide minerals such as magnetite were identified in any of the corrosion samples. However, the high background around 45°2θ in the diffraction pattern of the oriented wire 30C sample may be caused by X-ray amorphous material (Figure 5-1). Other minerals identified in MX-80 and both corrosion samples included quartz (3.34 Å), cristobalite (4.02 Å) and feldspars (sharp peaks at 3.16–3.20 Å) and in Kutch 8939, calcite (3.02 Å) and hematite/goethite (2.69 Å).

5.3 XRD anoxic

XRD patterns of all five samples (MX-80, wire 30C, wire 50C, coupon 30C and coupon 50C bentonites) mounted in glass capillaries to exclude air are shown in Figure 5-4 and in Appendix 2. The d-value of the (001)-peak of the three samples studied in the first phase (MX-80, wire 30C and coupon 50C) is around 16 Å (Figure 5-4) indicating that the relative humidity was high, probably more than 70–80%. When the coupon 50C bentonite sample was

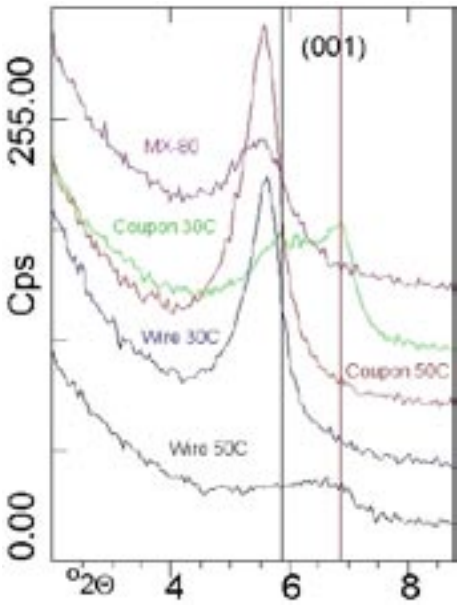

Figure 5-4. *XRD patterns of MX-80 and the four corrosion bentonites equilibrated in glove box and packed in glass capillaries. The black line indicates the position of d_{001} at 15 Å and the brown line at 12 Å.*

tested in air the d-spacing for the (001) peak dropped to 12.5 Å (i.e. similar to the oxic measurements). In the second set of samples (wire 50C and coupon 30C) the relative humidity inside the glass capillaries was apparently lower, giving smaller basal spacings. The reason for the high humidity of the first set of samples may be that because the samples were encased in glass they reached equilibrium with the trapped atmosphere such that the local humidity was high. The nitrogen in the glove box had a relative humidity in the range 30–40%, but it could have increased when water samples were present; in addition, some humidity is produced when the oxygen scrubber columns are regenerated by passing argon-hydrogen mixture over the copper catalyst columns, which remove oxygen from the recirculated nitrogen in the glove box.

In addition to quartz peaks, two moderately sharp and intensive peaks are seen in XRD patterns of the wire 50C and coupon 30C bentonites (Appendix 2). They are probably due to impurities and so well resolved because the overall intensities are very low (less than 100 counts/second) due to the random orientation and, in the case of the wire samples, the crumbly nature of the bentonite.

5.4 Laser Raman spectroscopy

This method was used for the investigation of corrosion products on the surface of cast iron and carbon steel coupons in contact with bentonite as well as of the wires. Hematite, magnetite and goethite were identified on the surface of the coupons (Figure 5-5), indicating that some aerobic oxidation of the surface had occurred, either during preparation of the specimens for the corrosion experiments, or after sealing in the plastic box used for the Raman measurements, which may not have been as air tight as the glass capillaries used for the wire measurements. On the wires, only magnetite could be detected, although the spectra were quite weak (Figure 5-6). Spectra were also obtained for bentonite (Kutch, MX-80, coupon-bentonite and wire-bentonite). The spectra for the bentonite samples were fairly weak and did not correspond to any of the common iron oxides, but they did agree with literature data for Raman of Na-montmorillonite /Bishop and Murad 2004/. The main bands are due to vibrations within the SiO_4 unit.

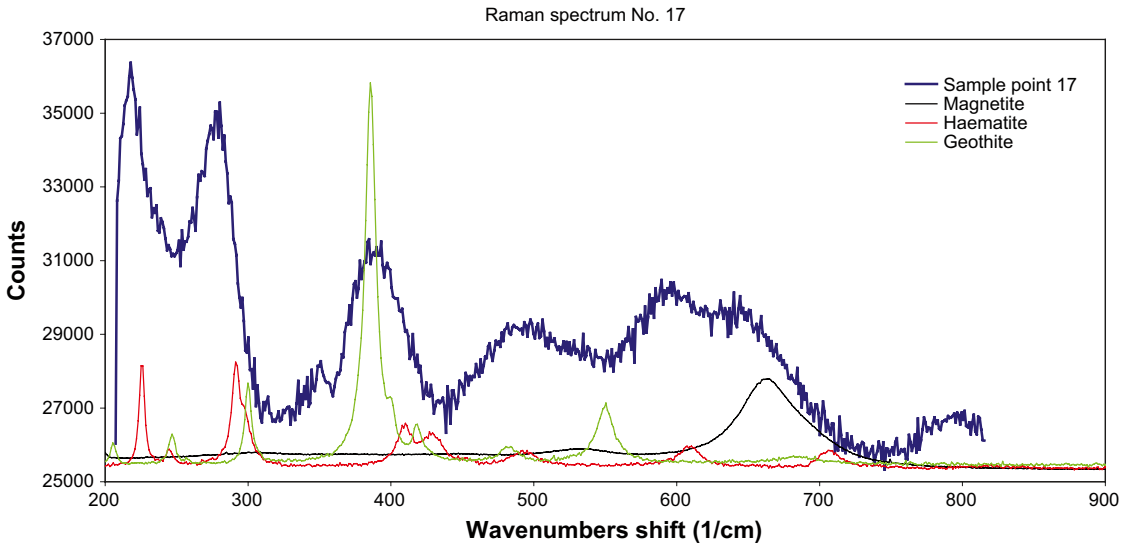

Figure 5-5. *Typical laser Raman spectrum of corrosion product found on the surface of cast iron and carbon steel coupons kept in contact with compacted bentonite for 356 days at 50°C in anaerobic conditions. The reference spectra of iron oxides magnetite, hematite and goethite are included.*

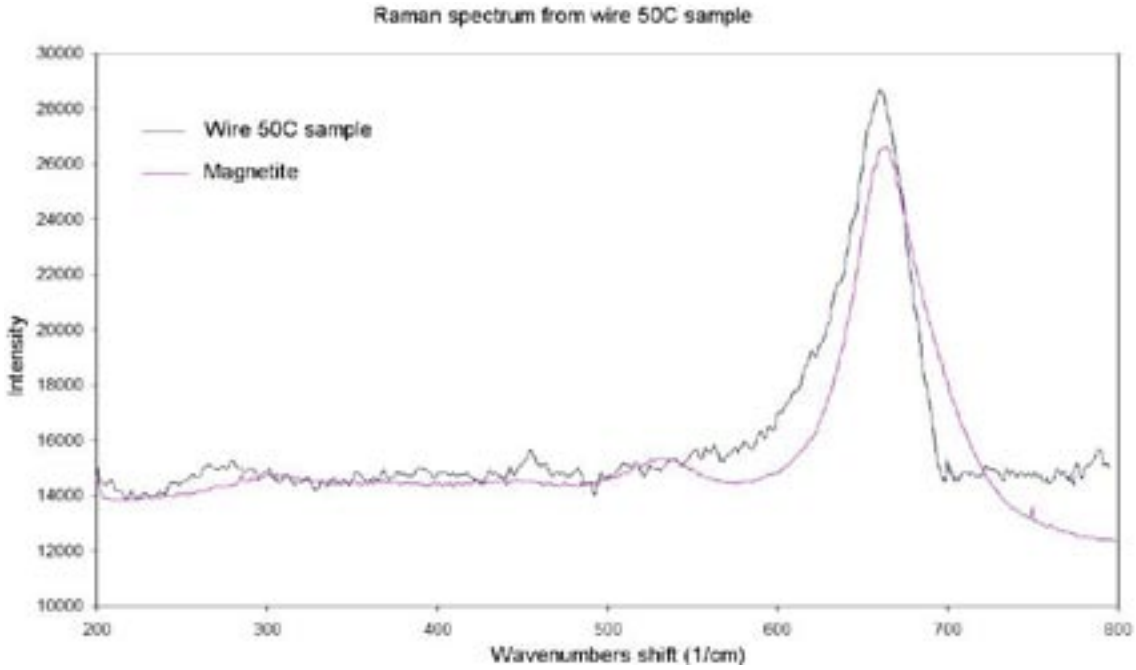

Figure 5-6. *Laser Raman spectra of wire 50C bentonite and standard magnetite.*

5.5 SEM-EDX and SEM-EPMA

The surfaces of the wires removed from the bentonite matrix were relatively clean (Figure 5-7) with little evidence of corrosion product; this is consistent with the weak Raman spectrum that was obtained from the surface of the wires. The EDX analysis (Figure 5-7) shows that the Fe content in bentonite close to the wire surface was high (up to 27 wt%). A closer look at the steel surface shows rectangular forms (Figure 5-8; Appendix 3) that are probably due to etching. Corrosion during the test in bentonite has followed the crystallographic structure of the steel. For comparison a sample of freshly pickled steel wire was examined in the SEM and the surface did not display the type of etching shown in Figure 5-7, suggesting that the features seen in Figure 5-7 were generated by corrosion in the bentonite.

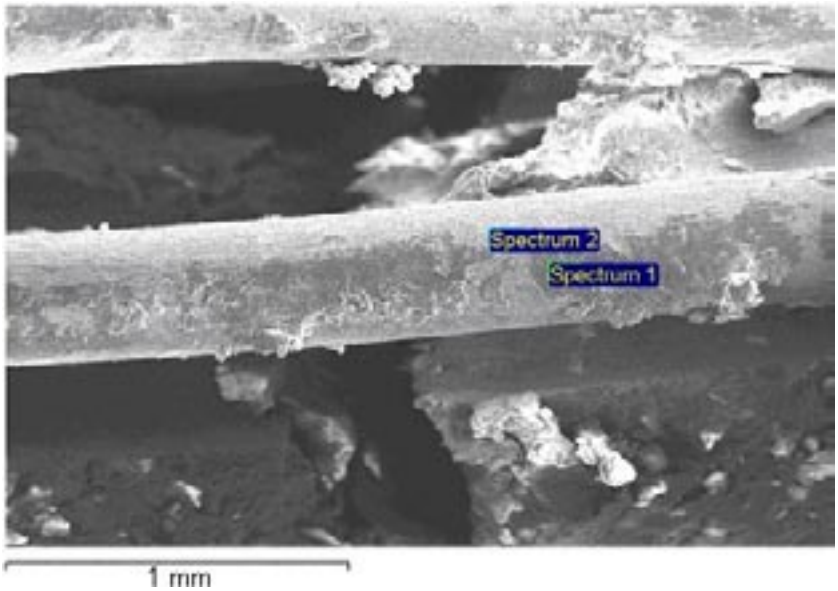

Figure 5-7. *SEM image of a piece of wire removed from compacted bentonite after 829 days at 30°C in anoxic conditions. EDX analyses in wt%:*

	O	Na	Mg	Al	Si	Cl	Ca	Mn	Fe	Total
Spectrum 1	42.46	1.21	1.04	7.19	20.49	0.34	0.29		26.98	100
Spectrum 2	4.86			0.62	1.60			0.44	92.98	100

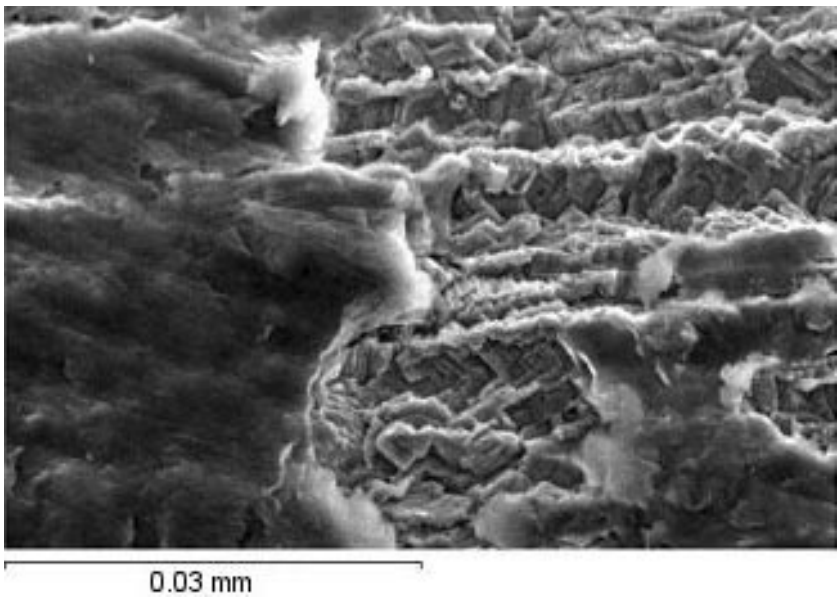

Figure 5-8. *SEM image of bentonite adhering to the surface of wire (829 days, 30°C). The smooth surface on the left hand side is bentonite and rectangular etch figures can be seen on the surface of steel wire. EDX analyses are given in Appendix 3.*

Examples of the results of electron microprobe analyses undertaken using a Jeol 880 Superprobe are presented in Figures 5-9 to 5-11 and in Appendix 4. Results of point analyses of the wire 30C bentonite are presented in Table 5-1 and the analysed points are marked in Figure 5-11. An enrichment of iron can be seen in the bentonite in the contact zone with cast iron/carbon steel in both coupon and wire bentonites. The iron content gradually decreased with distance from the contact zone. The thickness of the affected zone for the coupon samples varies from 0.1 to 1.25 mm.

Table 5-1. SEM-EPMA point analyses of the bentonite in contact with carbon steel wire at 30°C (in wt%). The locations of the point analyses are marked in Figure 5-11. The chemical composition of MX-80 from Table 5-9 is included for comparison. The element contents are recalculated as oxide percents, with iron as FeO.

No.	Na_2O	MgO	Al_2O_3	SiO_2	Cl	K_2O	CaO	TiO_2	FeO	Total
1	2.7	2.4	20.8	56.3	0.2	0.1	0.5	0.1	8.2	91.4
2	3.1	2.3	21.3	60.8	0.5	0.2	0.9	0.1	6.4	95.7
3	3.0	2.4	22.6	59.6	0.6	0.1	0.9	0.1	6.3	95.9
4[c) d)]	2.8	2.2	20.2	58.1	0.6	0.9	1.0	0.1	4.9	91.1
5[a)]	1.5	1.5	11.8	54.7	0.7	0.2	0.9	0.1	3.4	75.1
6	2.3	2.0	19.6	58.9	0.5	0.2	1.1	0.1	7.3	92.0
7[b)]	1.5	1.9	16.8	52.0	0.3	0.1	0.6	0.1	12.7	86.0
8[c)]	2.1	1.8	19.3	53.6	0.2	0.1	0.6	0.1	12.9	90.8
9[b) d)]	2.3	2.5	20.8	59.3	0.2	0.1	0.7	0.1	8.7	94.8
10	2.4	2.4	22.0	57.4	0.2	0.2	0.6	0.1	9.4	94.9
11[c)]	3.8	3.2	22.4	56.9	3.0	0.4	0.7	0.1	4.4	95.0
MX-80	1.7	2.5	19.1	54.6	0.0	0.6	1.3	0.1	3.1	83.0

[a)] P_2O_5 0.1%; S, 0.1%; [b)] MnO 0.1%; [c)] CuO 0.1%; [d)] BaO 0.1%.

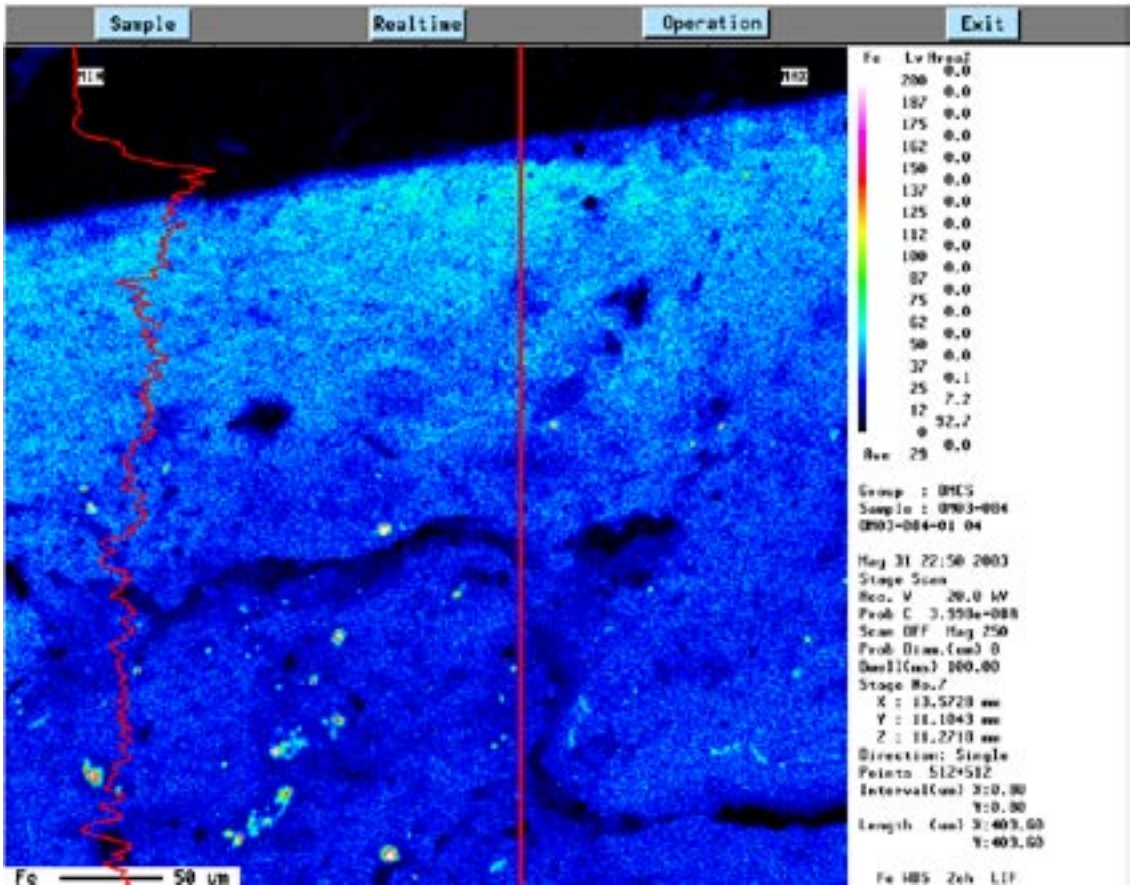

Figure 5-9. *EPMA-map of the distribution of Al, Fe, S, Cl, Si and Ca in the coupon 30C bentonite.*

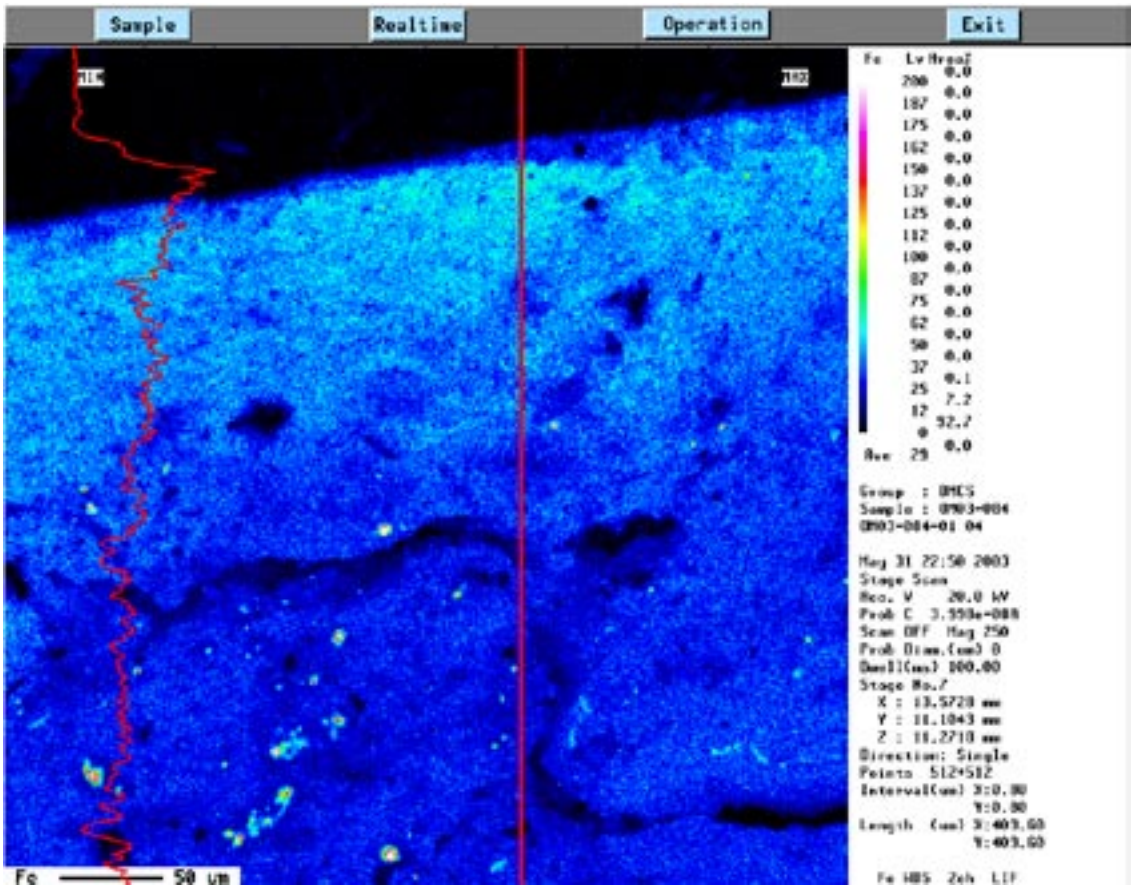

Figure 5-10. *EPMA map of the distribution of Fe with profile (left) in the bentonite in contact with a carbon steel coupon for 356 days at 50°C. The vertical line indicates the location of the profile.*

In the EPMA maps of the distribution of Fe, a number of small bright areas were detected (Figures 5-9 to 5-11). These correspond to areas with high sulphur content, showing the position of small iron sulphide crystals (Figure 5-9). There were indications of other mineral inclusions present in the clay as shown by areas of slightly increased back-scattered electron signal, but these were randomly distributed, and showed no obvious relationship with the contact with the metal. The only element that did show such a relationship was calcium, which showed higher concentrations at the surface as well as the occasional distinct mineral grain (Figure 5-9).
A similar section of the sample in contact with the cast iron did not show much although it was possible to see a slight darkening of the clay visually.

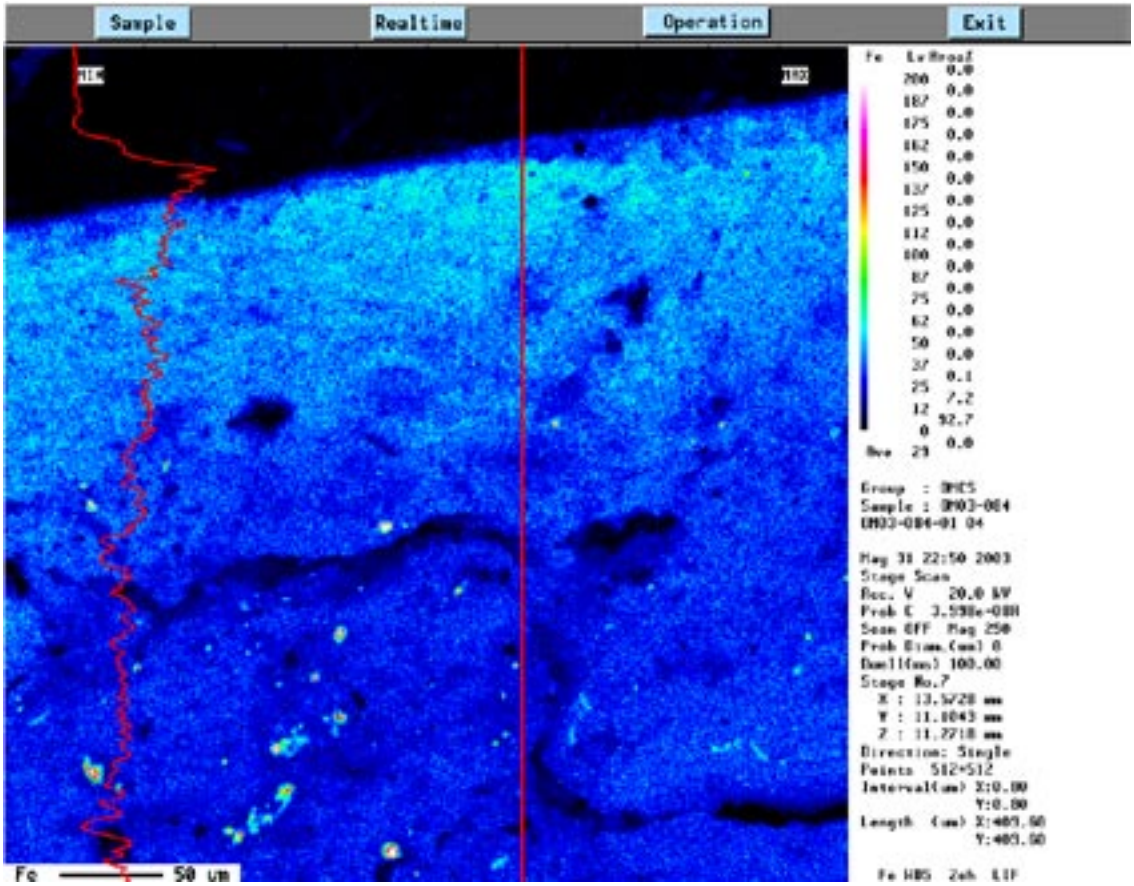

Figure 5-11. *EPMA map of the distribution of Fe in the wire 30C bentonite. The sites of point analyses are marked. See Table 5-1.*

5.6 Mössbauer spectroscopy

Mössbauer data of all four samples are presented in Table 5-2 and in Figure 5-12. Isomer shifts, quadrupole splittings and full linewidths as well as oxidation states and site symmetries are given. The interpretation of the spectra, provided by Dr. A.M. (independent corrosion consultant) is as follows.

Specimens MX-80 and Kutch 8939

The Kutch bentonite is clearly much more highly oxidised, as it contains no detectable Fe^{2+} – this would be very easily seen at c-2.5 mm/sec. The "extra" iron would appear to be present as a separate phase of Fe^{3+} oxide/hydroxide, rather than substituted in the clay mineral lattice. The magnetic splitting (6 lines, corresponding to an internal magnetic field of 510 kOe) is the result of cooperative magnetism associated with close contact between iron ions in a lattice such as an oxide overcoming thermal motions that lead to relaxation of the electron spin orientations. The rather broad lines could be the result of a range of particle sizes, and are not uncommon in iron oxides/hydroxides formed at low temperatures. The remaining Fe^{3+} is probably substituted in the clay lattice in similar octahedral positions. Since the Fe^{3+} is present as an impurity element in what is anyway a range of silicate minerals, the quadrupole splitting may vary somewhat, giving a fitted line width that is broader than for the Fe^{2+} present.

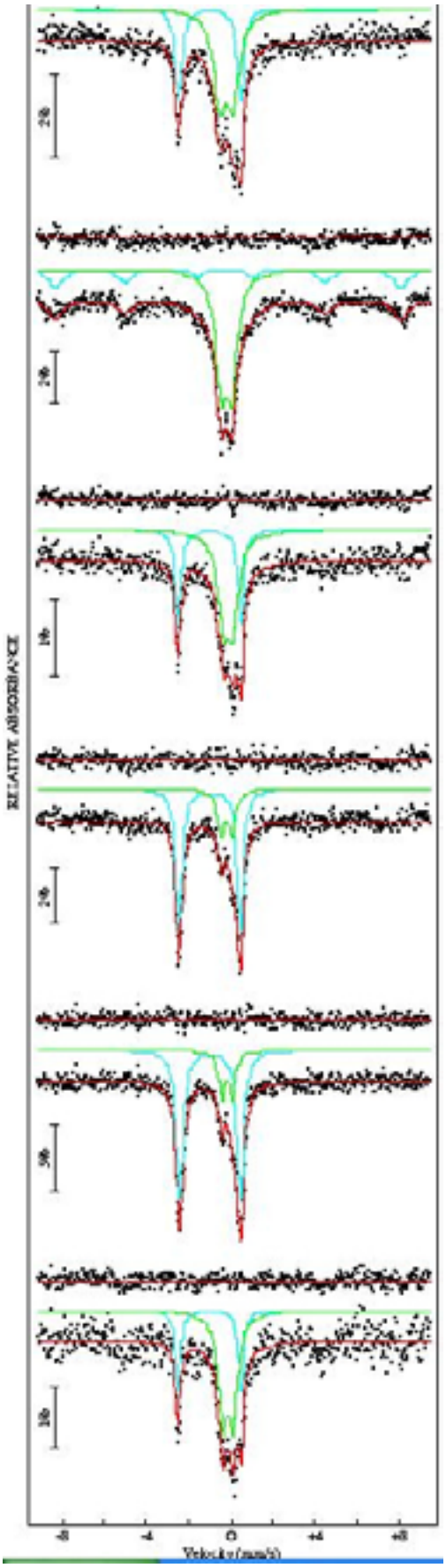

Figure 5-12. *Mössbauer measurements for bentonite clay samples. From top: MX-80, Kutch 8939, coupon 50°C, wire 30°C, wire 50°C and coupon 30°C bentonites.*

Table 5-2. Mössbauer data of MX-80, the four corrosion bentonites and Kutch 8939.

	MX-80		Coupon 30C[a]		Coupon 50C	
Site	**1**	**2**	**1**	**2**	**1**	**2**
δ (mm/s)	0.451	1.248	0.418	1.250	0.368	1.255
Δ (mm/s)	0.632	2.952	0.555	3.017	0.465	2.995
Γ (mm/s)	0.709	0.370	0.494	0.317	0.618	0.308
BHF (kOe)						
Area (%)	63.9	36.1	49.4	29.9	64.9	35.1
Oxidation state and site symmetry	Fe^{3+} (oh)	Fe^{2+} (oh)	Fe^{3+} (oh)	Fe^{2+} (oh)	Fe^{3+} (oh)	Fe^{2+} (oh)

δ = Isomer shift; Δ = Quadrupole splitting; Γ = Full linewidth; (oh) = Octahedral.
[a] in sample coupon 30C three more sites were measured (6.8, 5.3 and 8.6%, respectively) but they are very weak. Sites 1 and 2 give a Fe^{3+}/Fe^{2+} ratio 62.3/37.7.

	Wire 30C		Wire 50C		Kutch 8939	
Site	**1**	**2**	**1**	**2**	**1**	**2**
δ (mm/s)	0.443	1.253	0.421	1.231	0.451	0.439
Δ (mm/s)	0.525	2.915	0.506	2.894	0.513	0.144
Γ (mm/s)	0.392	0.347	0.355	0.385	0.620	0.773
BHF (kOe)						51.0
Area (%)	25.9	74.1	22	78	69.0	64.9
Oxidation state and site symmetry	Fe^{3+} (oh)	Fe^{2+} (oh)	Fe^{3+}	Fe^{2+}	Magnetic iron	Fe^{3+} (oh)

δ = Isomer shift; Δ = Quadrupole splitting; Γ = Full linewidth; (oh) = Octahedral.

Coupon 50C bentonite

The scatter in this spectrum is significantly greater than in the other spectra, so the quality of the data may not be so good. It seems likely that the differences between the spectra of MX-80 and the coupon 50C bentonite are not significant. The almost identical ratios of Fe^{2+}/Fe^{3+} could have one of two interpretations:

1) the materials are essentially identical, with no extra iron from corrosion products,
2) there is extra corrosion product, but in a similar chemical environment to that in the original bentonite; this would imply that the corrosion products probably released as ions, then absorbed, and did not form a separate oxide/hydroxide phase.

The very similar parameters for Fe^{2+} and the relatively narrow linewidths in MX-80 and the coupon 50C bentonite support this view. However, it is not certain what would happen to any $Fe(OH)_2$ formed during the course of the experiment. The Mössbauer parameters might be the same as for Fe^{2+} in bentonite, by coincidence. However, the $Fe(OH)_2$ might decompose to magnetite, though there is no sign of it in the spectrum.

Wire 30C bentonite + wires

Perhaps the most significant feature of the spectrum is the large Fe^{2+}/Fe^{3+} ratio. The parameters of Fe^{2+} are almost identical with those in MX-80 and the wire 50C bentonite, suggesting that the Fe^{2+} ions are in a similar environment. The Fe^{3+} parameters are similar to those in MX-80 and Kutch 8939, though the line width is smaller. It is not clear how significant this is, and it might just reflect a smaller range of quadrupole splitting. These observations suggest one of three possibilities:

1) corrosion of the iron in the matrix has reduced some of the Fe^{3+} in octahedral positions, possibly accompanied by additional substitution by Fe^{2+} ions in the bentonite lattice,
2) there is additional substitution of Fe^{2+} in the bentonite lattice; this increases the Fe^{2+}/Fe^{3+} ratio without affecting the Fe^{3+} present,
3) the extra Fe^{2+} from corrosion is in a similar position chemically/electrically to that in the bentonite lattice, and so cannot be distinguished from it.

The Mössbauer spectra did not match any of the known spectra for common iron corrosion products /Vértes and Czakó-Nagy 1989/. Fe^{2+} corrosion species separate from substituted Fe^{2+} in bentonite may exist, but if so, their Mössbauer parameters are almost identical with those of Fe^{2+} in the MX-80 bentonite. It might be possible to demonstrate this by running a Mössbauer spectrum at a different temperature (e.g. 25°C), as the temperature dependence of the quadrupole splittings and isomer shifts might well be different, leading to better fits with two Fe^{2+} species.

5.7 FTIR

Infrared absorption bands in the OH-bending frequencies between wavenumbers 800 cm^{-1} and 1,000 cm^{-1} reflect the composition of octahedral montmorillonite sheets. In MX-80 the AlAlOH band at ca. 920 cm^{-1} is strong and the $AlFe^{3+}OH$ band at ca. 880 cm^{-1} as well as the AlMgOH band at ca. 850 cm^{-1} are weaker (Figure 5-13, Table 5-3) indicating the dominance of aluminium in the octahedral sheets. The spectra of both coupon bentonites are similar to that of MX-80 (Figure 5-13). FTIR-spectra of wire bentonites that were recorded immediately after removing the samples from the glove box differ from the spectrum of MX-80. The $AlFe^{3+}OH$ band at 880 cm^{-1} is very small or non-existent and the band at 840 cm^{-1} is bigger than in MX-80 (Figures 5-14 and 5-15). The disappearance of the $AlFe^{3+}OH$ band upon reduction of a ferruginous smectite (nontronite) was reported also by /Komadel et al. 1999/ and /Manceau et al. 2000/. When the powdered sample was allowed to oxidize in air, the $AlFe^{3+}OH$ band enlarged and the 840 cm^{-1} band diminished (Table 5-3). At the same time the bluish green colour of the powder turned olive green, indicating partial oxidation of iron. It is apparent that Fe^{3+} in the octahedral montmorillonite sheets was reduced to Fe^{2+} in the presence of metallic iron. The FTIR band at 840 cm^{-1} in the reduced wire bentonites cannot be assigned to AlMgOH only but also to $AlFe^{2+}OH$. According to /Farmer 1974/ the $MgFe^{3+}OH$ and the $Fe^{2+}Fe^{3+}OH$ bands coincide. The $AlFe^{2+}OH$ band is not mentioned by Farmer. When the wire 30C bentonite sample was mixed with deionized water in air, in order to separate the clay fraction, the sample was fully oxidized and the FTIR spectrum was similar to that of MX-80 (Figure 5-13). No bands due to any iron oxide mineral could be observed in any of the corrosion bentonites. The FTIR spectrum of Kutch 8939 closely resembles that of MX-80.

Table 5-3. Areas of three FTIR bands calculated as % of total.

Sample	AlAlOH	$AlFe^{3+}OH$	$AlMgOH/AlFe^{2+}OH$
MX-80	60	20	20
Coupon 30C	64	18	18
Coupon 50C	63	27	10
Wire 30C	69	2	29
Wire 30C, oxidized	56	17	27
Wire 50C	58	0	42
Wire 50C, partly ox.	59	4	37

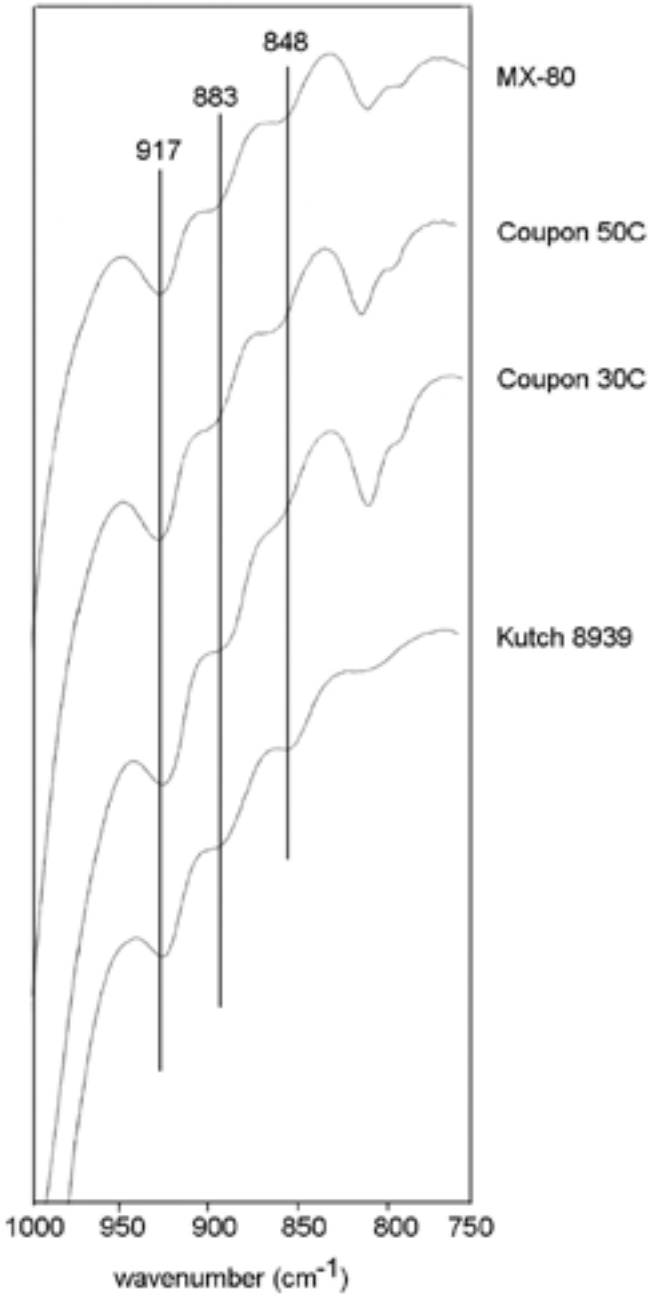

Figure 5-13. *Part of the IR spectra of MX-80, the coupon 50C and coupon 30C corrosion samples as well as the reference sample Kutch 8939. The positions of the AlAlOH (917 cm^{-1}), AlFe(III)OH (883 cm^{-1}) and AlMgOH (848 cm^{-1}) bands are marked. Two additional bands in the spectra of MX-80 and the two corrosion samples at 798 and 778 cm^{-1} are due to quartz and opaline silica.*

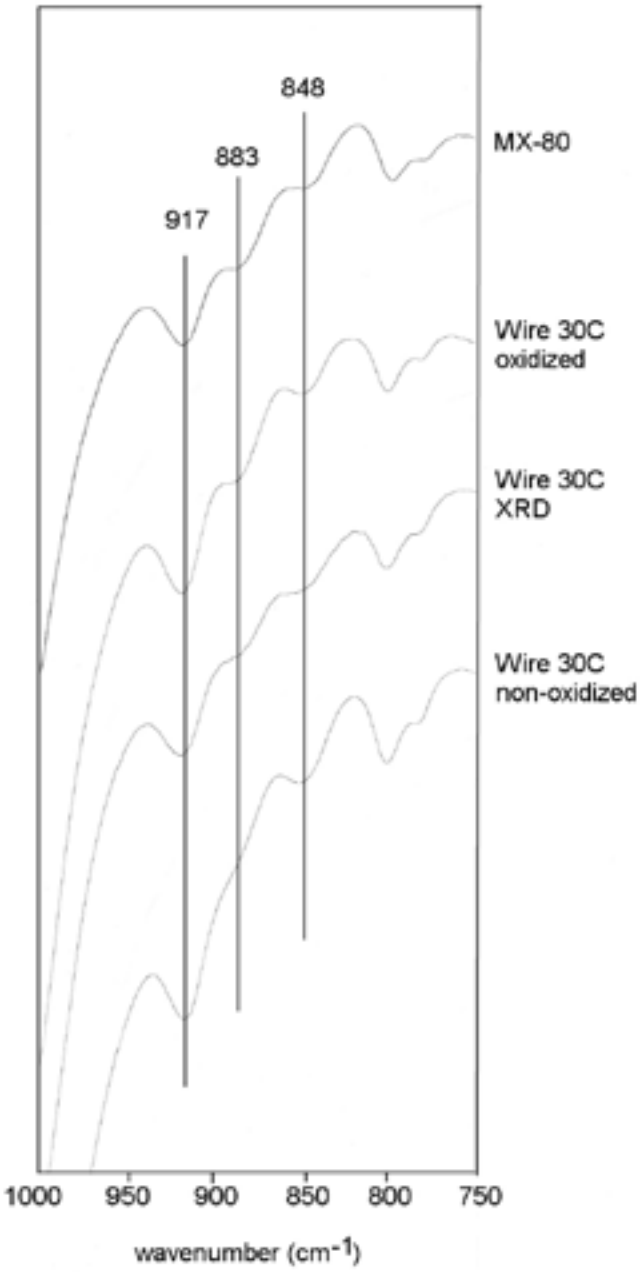

Figure 5-14. *Part of the FTIR spectra of MX-80 and the wire 30C corrosion sample in three phases of oxidation. The sample labelled non-oxidized was pulverized, the pellet pressed and the spectrum recorded as soon as possible after removing it from glove box. The sample labelled XRD was fractionated, mounted and dried for XRD in a nitrogen-purged glove box. The bluish green colour of the material remained unchanged for weeks in air. The FTIR spectrum was recorded after 6 weeks in air. The sample labelled oxidized was fractionated in deionized water and dried at 80°C. The colour turned brown within one hour. The positions of the AlAlOH (917 cm^{-1}), AlFe(III)OH (883 cm^{-1}) and AlMgOH (848 cm^{-1}) bands are marked. Bands at 798 and 778 cm^{-1} are due to quartz and opaline silica.*

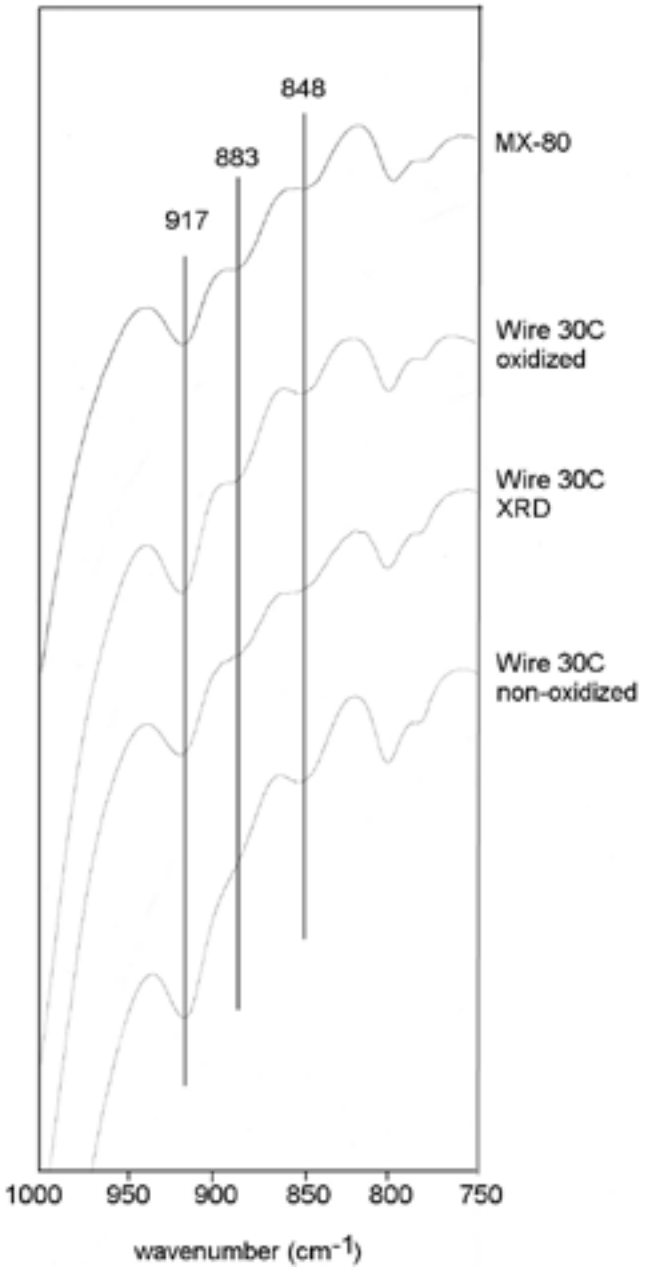

Figure 5-15. *Part of the IR spectra of MX-80 and the wire 50C corrosion sample in two phases of oxidation. The sample labelled non-oxidized was pulverized, the pellet pressed and the spectrum recorded as soon as possible after removing it from the glove box. The pulverised material was bluish green. The sample labelled 4 days in air had turned olive green indicating partial oxidation of Fe(II). The positions of the AlAlOH (915 cm^{-1}), AlFe(III)OH (882 cm^{-1}) and AlMgOH (844 cm^{-1}) bands are marked. Bands at 798 and 778 cm^{-1} are due to quartz and opaline silica.*

5.8 Exchangeable cations and CEC

CEC and the exchangeable cation concentrations determined by extraction into 0.1 M $BaCl_2$ solution are given in Table 5-4. The extractions were carried out in two batches, the first in September 2004 (Set 1 in Table 5-4) and the second in December 2004 (Set 2 in Table 5-4). The first batch was also extracted in air (Table 5-5).

Differences were observed between the two batches in the CEC values, determined as the difference between the Ba concentration in solution before and after the extraction In this method only a small portion (6–10%) of the Ba added is sorbed by the bentonite, which means that if errors are introduced in the concentration measurements, they will accumulate in the calculations. The CEC values obtained for the first batch are probably more reliable than the values obtained for the second batch, because the first determination of CEC for MX-80 matches the expected value, 75–80 $cmol^+/kg$, reasonably well.

Additional CEC determinations were performed using Ba-133 (Table 5-6) and Cu(II)-triethylenetetramine (Table 5-7) as displacing cation/cation complex. The results of these measurements suggest that the CEC of the coupon bentonite samples was essentially unchanged after the corrosion tests, whereas the CEC of the wire 50C bentonite sample was significantly reduced. Similarly, the corrected sum (see below) of the exchangeable cations for the coupon samples (Table 5-4) matches the CEC of MX80, but for both the wire bentonite samples a significant loss in CEC is indicated. Oxidation of the bentonite appears to increase the ease with which Na and Mg were released into the extractant (Table 5-5).

In addition to the exchangeable cations listed in Tables 5-4 and 5-5, an insignificant amount of iron, equivalent to 0.03–0.09 $cmol^+/kg$, was extracted into $BaCl_2$ solution from the wire bentonite samples. The extractable amount is in no way correlated to the amount of iron incorporated, which corresponds to an addition of between 6.6 and 8.7% extra Fe to MX80 (cf. chemical data in Table 5-10). The quantity of Fe(II) required to saturate all exchange sites in MX80 is less than 3%, and this comparison makes it evident that the incorporation of iron is far in excess of the CEC. And yet, at least half of the exchange sites seem to be occupied by a remnant cation pool of Na, K, Ca and Mg.

Table 5-4. Results of cation exchange capacity (CEC) and exchangeable cations analyses. The extractions were carried out using 0.1 M $BaCl_2$-solution in an inert atmosphere. The sum of exchangeable Ca, K, Mg and Na based on the ICP-AES analysis of the extract is also given. The wire 30C bentonite sample was extracted with pieces of wire still present and the bentonite sample weight was calculated using the original ratio wire/bentonite. In the case of the wire 50C bentonite sample the pieces of wire were removed before extraction. Samples included in Set 1 was extracted in September 2004, samples in Set 2 in December 2004.

N_2	Sample	CEC	Ca	K	Mg	Na	Sum
Sample	size, g	$cmol^+/kg$			$cmol^+/kg$		
Set 1							
Coupon 50C 1	0.58784	64.3	18.5	1.28	6.13	60.1	85.9
Coupon 50C 2	0.61436	68.2	18.6	1.25	6.10	59.2	85.2
Wire 30C 1	0.7640	34.6	9.28	0.62	3.34	30.9	44.1
Wire 30C 2	0.72059	59.6	10.3	0.73	4.12	34.1	49.2
MX-80 1	0.41789	84.4	30.5	1.73	9.24	49.9	91.3
Kutch 8939	0.42285	109	46.2	0.57	21.1	45.7	114
Set 2							
Coupon 30C 1	0.6356	111	15.9	1.13	6.93	61.3	85.3
Coupon 30C 2	0.6440	90.2	16.1	1.49	6.93	61.4	85.9
Wire 50C 1	0.6365	81.6	11.8	0.87	1.65	45.2	59.5
Wire 50C 2	0.5734	79.1	11.9	0.79	1.59	45.4	59.7
MX-80 2	0.4322	114	24.8	1.88	9.13	47.5	83.8
MX-80 3	0.4415	160	24.8	1.83	9.27	48.3	84.2

Table 5-5. Cation exchange capacity and exchangeable cations. The extractions were performed in air, all other details are as described for Table 5-4.

Air Sample	Sample size, g	CEC cmol$^+$/kg	Ca	K	Mg	Na	Sum
			cmol$^+$/kg				
Coupon 50C 1	0.61915	74.4	18.2	1.25	6.15	60.8	86.4
Coupon 50C 2	0.63988	63.9	18.2	1.27	6.17	60.2	85.8
Wire 30C	0.66745	69.4	12.0	0.86	5.98	43.9	62.7
MX-80 1	0.43902	88.5	29.6	1.64	9.12	48.5	88.9
MX-80 2	0.43631	78.5	29.5	1.64	9.05	48.5	88.6
Kutch 8939 1	0.43130	108	47.4	0.55	20.6	45.2	114
Kutch 8939 2	0.43914	105	47.5	0.55	20.7	45.4	114

Table 5-6. Cation exchange capacity of three samples determined using Ba-133. 0.0235 M $BaCl_2$-solution was used to ensure high enough sorption. Accuracy of the results on 96% level of confidence is ca 8%.

Sample	Sample size, g	Sorption, %	CEC, cmol$^+$/kg
Coupon 30C	0.662	29.6	71.0
Wire 50C	0.739	25.0	54.0
MX-80	0.483	20.1	67.0

Table 5-7. Cation exchange capacity (CEC, cmol$^+$/kg) determined using Cu(II)-triethylene-tetramine. The extractions were carried out in an inert atmosphere Sample Wire 50C ox was slightly oxidized when the determination was done.

Sample	CEC cmol$^+$/kg	
	1	2
MX-80	71	74
Coupon 30C	76	76
Coupon 50C	77	80
Wire 30C	75	71
Wire 50C ox	56	61
Wire 50C	58	63

As can be expected, equilibration with the synthetic groundwater (0.54 M NaCl and 0.01 M Na-carbonate) during the corrosion experiments caused cation exchange in the bentonite, leading to an increase in the Na/Ca ratio. Some of the extra Na in the corrosion samples was extracted from NaCl that had precipitated on drying. The residual sodium chloride content in the bentonite was determined by analysis of the water used for the grain size fractionation of one of the corrosion samples for XRD. The amount of NaCl dissolved in deionised water was ca 4 mg/g bentonite, which is comparable with the average NaCl content indicated in the EPMA point analysis, 6.6 mg NaCl/g bentonite; (cf. 5.5). Thus, the contribution of Na due to dissolution of residual sodium chloride is in the range 7–11 cmol$^+$/kg. If corrections are made for this contribution, the relative proportion of sodium increased from ca. 55% in MX80 to ca. 68% in the coupon samples. The sodium proportion of the remnant cation pool in the wire bentonite samples is almost the same, ca 65%. The proportion of calcium and magnesium decreased correspondingly.

5.9 TEM-EDS

Platy montmorillonite particles with ragged and sometimes curled edges were observed with a transmission electron microscope (Figure 5-16). Their diameters ranged from 1.5 µm to 15 µm. The biggest particles were found in the strongly aggregated black wire 30C bentonite samples. In addition, rounded quartz particles were observed in MX-80 and the corrosion bentonites and feldspar grains were present in the coupon 30C (plagioclase) and wire 50C bentonite samples (plagioclase and K-feldspar). Electron diffraction patterns of all montmorillonite particles show a series of rings (Figure 5-16) indicating turbostratic disorder of stacking. Only when very thin particles were studied was a faint indication of dots seen. The calculated d-values in all the montmorillonite patterns were 4.36–4.44 Å (strong), 2.51–2.57 Å (strong), 1.65–1.67 Å (weak), 1.48–1.50 Å (moderate) and 1.27–1.29 Å (weak) and they correspond to XRD peaks with d-values 4.50 Å (hkl 110.020), 2.57 Å (hkl 006), 1.70 Å (009), 1.49 Å (060) and 1.28 Å (weak).

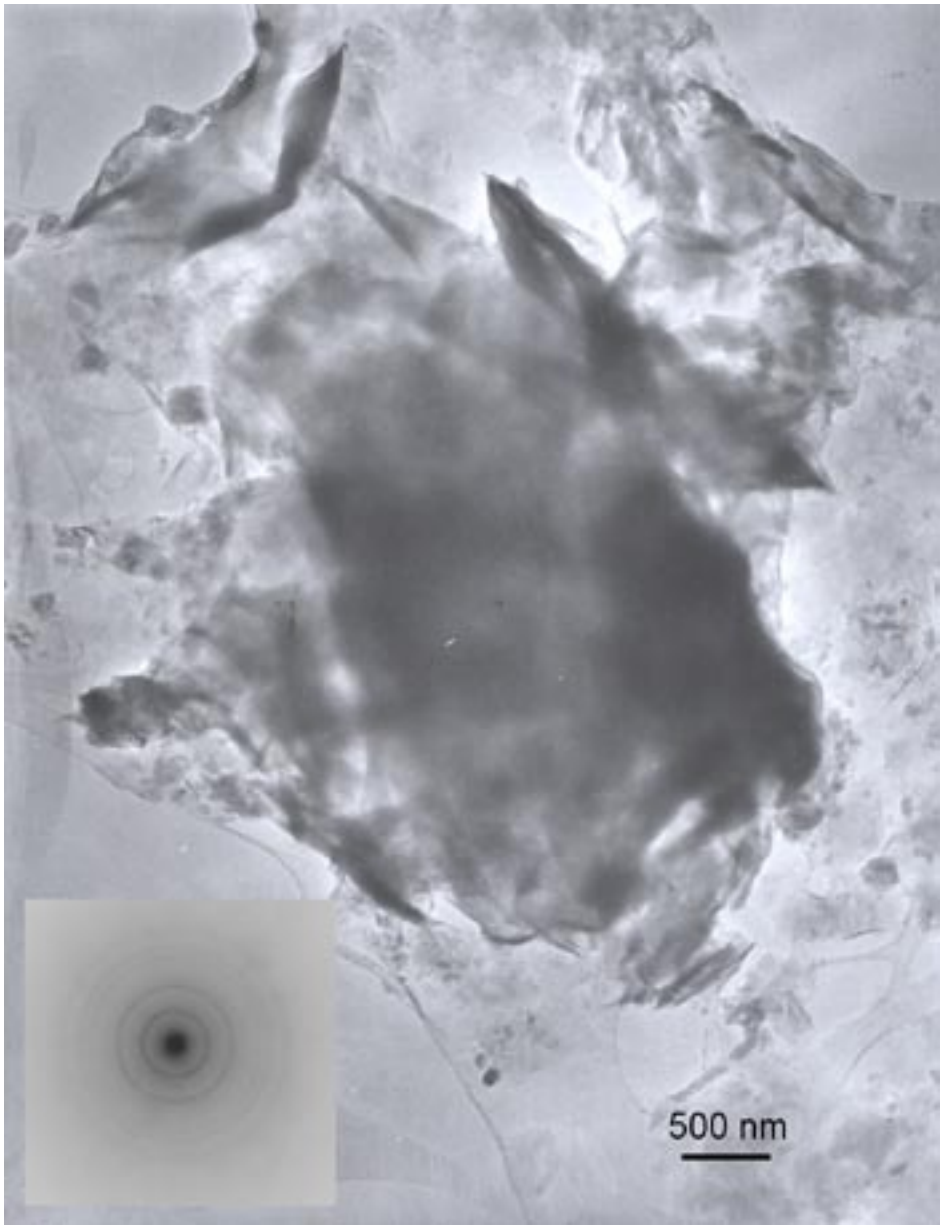

Figure 5-16. *TEM-photo of a montmorillonite aggregate in sample coupon 50C. The small photo in the lower left corner is an electron diffraction pattern of the aggregate. The rings outwards from the origin correspond to d-values 4.5 Å, 2.57 Å (both strong), 1.70 Å (weak), 1.49 Å (moderate) and 1.28 Å (weak).*

Unfortunately, the dots and rings with d-values over 10 Å were masked by the origin so that d_{001} values could not be calculated. The characteristic electron diffraction patterns of quartz and feldspar crystals were recorded.

EDS analyses were performed at 2 to 7 points on each montmorillonite grain and 5 to 10 grains per sample were photographed and analysed. The average compositions and standard deviations are given in Table 5-8. The average iron content was not significantly higher in the coupon 30C and coupon 50C bentonite samples than in fresh MX-80 (i.e. ~ 2 wt%). However, the iron content of montmorillonite grains in the coupon bentonites, showed more variation than the iron content of grains in MX-80. The calculated structural formulae of montmorillonite in MX-80 and the two coupon bentonites closely resembled each other: $Si_{4.00}(Al_{1.60–1.63}Fe_{0.13–0.14}Mg_{0.23–0.26})O_{10}(OH)_2$. The average compositions of octahedral sheets with the corresponding standard deviations are given in Table 5-9. One grain in the coupon 50C bentonite showed diverging structural formula and higher Fe-content than the other four grains measured. Apparently, some additional iron (e.g. in the form of an oxide coating or adsorbed Fe(II)) is present in the grain. Specimens for TEM were taken as close to the brownish black contact zone in the coupon bentonite samples as possible.

The highest iron contents were found in the wire 30C and wire 50C bentonite samples.

A significant variation in the iron content measured in individual grains is evident (Table 5-8) and even the iron content measured in different parts of single grains showed a considerable variation (e.g. wire 50C, grain 2, 5.6–8.8% Fe; grain 5, 10.0–16.4% Fe). The grains were thick and electron dense, indicating a high iron content. It is, however, not possible to say whether the additional iron was present as Fe(II) substituting for Na^+ or Ca^{2+} in the interlayer positions or as an iron oxyhydroxide present on the surface of the montmorillonite crystals. No iron oxyhydroxide particles could be detected with TEM in any of the wire bentonites. In the clay fraction of the wire 30C bentonite sample the iron content was lower than in the bulk sample (Table 5-8). Apparently, some iron was removed during the grain size fractionation.

The Indian Kutch 8939 bentonite contains the iron oxides hematite and goethite and the average iron content of the montmorillonite aggregates was 5.4%. The standard deviation was high in this sample as well and the iron content varied considerably between each measurement.

Table 5-8. Average composition in wt% and standard deviation of smectite aggregates determined with TEM-EDS. The number of point analyses is in parentheses.

Sample	Si %	Al %	Fe %	Mg %	Ca %	Na %	K %
MX-80	38.98	13.69	2.04	1.56	0.19	0.15	0.06
Stdev (17)	2.91	2.21	0.64	0.66	0.09	0.15	0.05
Coupon 30C	34.43	14.37	2.57	1.95	0.40	0.34	0.09
Stdev (13)	1.95	1.13	0.42	0.29	0.11	0.31	0.03
Coupon 50C	39.20	12.87	2.50	1.45	0.44	0.13	0.08
Stdev (33)	3.00	2.79	1.45	0.54	0.30	0.03	0.04
Wire 30C	32.17	12.72	13.48	1.59	0.39	0.39	0.09
Stdev (13)	2.24	0.93	3.38	0.32	0.09	0.31	0.05
Wire 30C clay	36.63	10.03	5.97	0.96	0.23	0.01	0.01
Stdev (26)	4.02	2.27	2.46	0.39	0.20	0.01	0.01
Wire 50C	32.65	11.83	12.41	1.67	0.37	0.52	0.10
Stdev (19)	3.81	1.62	3.45	0.33	0.15	0.40	0.06
Kutch 8939	38.30	12.24	5.39	2.25	0.62	0.00	0.12
Stdev (23)	3.76	1.54	2.13	0.56	0.17	0.01	0.17

Table 5-9. Content of Al, Fe and Mg in the octahedral smectite sheets in MX-80 and two corrosion samples as well as in one Fe-rich aggregate in sample coupon 50C. N = number of measurements.

Sample	Al	Fe	Mg	N
MX-80	1.62	0.13	0.24	10
Stdev	0.05	0.01	0.04	
Coupon 30C	1.60	0.14	0.26	32
Stdev	0.04	0.02	0.04	
Coupon 50C	1.63	0.13	0.23	11
Stdev	0.03	0.03	0.03	
C50C Fe	1.57	0.27	0.16	3
Stdev	0.03	0.03	0.01	

Two determinations were omitted in the calculations for the corrosion samples because of high Si, K, Na or Ca values. Apparently, poorly crystalline SiO_2 as well as feldspars were present in some of the aggregates, in agreement with XRD analysis which identified cristobalite and quartz.

5.10 Total chemical composition

The total chemical composition of the four corrosion bentonites and two reference samples are presented in Table 5-10. Chemically, the coupon bentonites closely resemble MX-80. The only changes that occurred during the tests are a small increase in sodium content and a small decrease in calcium and magnesium contents. Cation exchange brought about by the synthetic ground water (NaCl + Na-carbonate) used in the tests is a logical explanation for these changes. The same conclusion was drawn from the CEC data (see section 5.8).

The difference between MX-80 and the two wire bentonites is more obvious. Compared to MX-80, the iron contents of the wire 30C bentonite and wire 50C bentonite samples were ca. 3.7 times (6.6 wt%) and 4.6 times (8.7 wt%) higher respectively. Similarly, the Mn content had increased considerably, by 3.9 times and 7.1 times in the wire 30C and wire 50C samples, respectively. The source of the extra iron and manganese is the corroding carbon steel wire. The higher Fe and Mn content of the wire 50C bentonite sample compared to the wire 30C bentonite sample can be explained by the higher test temperature and the somewhat longer test duration. Again, displacement of the interlayer cations by sodium from the background electrolyte explains the higher sodium and lower calcium and magnesium content of the corrosion samples.

The Kutch bentonite is characterised by a higher Fe, Mn and Ti content than the MX-80. It contains hematite, goethite and probably anatase.

Table 5-10. Total chemical composition. Si was determined using sodium peroxide fusion and the rest of the elements were determined using lithium metaborate fusion.

Sample	Si %	Al %	Fe %	Mg %	Ca %	Na %	K %	Ti mg/kg	Mn mg/kg	P mg/kg
MX-80	25.5	10.1	2.40	1.49	0.92	1.29	0.46	822	60.3	239
Coupon 30C	27.0	10.3	2.83	1.42	0.72	1.80	0.43	757	55.4	291
Coupon 50C	27.2	10.4	2.42	1.45	0.71	1.77	0.46	801	67.8	280
Wire 30C	24.4	9.39	9.03	1.30	0.48	1.45	0.42	712	237	278
Wire 50C	25.3	9.73	11.1	1.23	0.46	1.50	0.39	702	426	301
Kutch 8939	21.9	10.0	6.82	1.85	0.54	0.96	0.09	4,940	276	< 100

5.11 Swelling pressure and hydraulic conductivity

Swelling pressure and the hydraulic conductivity were determined for four different densities for each of the test materials (wire 30°C, wire 50°C, coupon 30°C and coupon 50°C). On delivery, the test material from the wire 50°C tests had a slight reddish colour compared to the other test materials indicating that it was slightly oxidized. Two additional non-oxidized wire 50°C samples were therefore tested. Two additional tests were run to extend the density range for the wire 30°C material.

The iron content of these samples, as revealed by the chemical analyses and the SEM and TEM analyses, was around 10% compared to 2.5% by weight in the original MX-80 material. The measured actual grain density in the wire samples was higher (2,850 kg/m^3) than that of the original MX-80 material (2,750 kg/m^3). The density differences correspond to an approximate increase in iron content from 2.5 wt% to 10 wt% if the iron is assumed to be in the form of magnetite, or to approximately 8 wt% if the iron is assumed to be present in the metallic form. The accuracy of the grain density determination is not good enough to distinguish between the two cases, but the density results are consistent with the measurements of total iron content.

The measured mean grain density and iron content, in the form of magnetite, were used to calculate the reduced dry clay density, in order to make a more correct comparison between results from the original MX-80 and clay exposed to corroding steel. The general trend is that there was a significant difference between the properties of the samples that had been in contact with corroding wires and the original MX-80 material (Figure 5-17).

In order to avoid the general accuracy problem with density determinations, especially with small test samples, the results are plotted as hydraulic conductivity versus swelling pressure in Figure 5-18. From this presentation it is obvious that all the bentonite samples exposed to corroding steel had an increased hydraulic conductivity compared to the original MX-80 material at the same swelling pressure. The difference is small for the coupon samples and no temperature effect can be noticed. In contrast, the wire samples show a significant difference as compared to the original MX-80 material and a marked temperature effect.

The increase in hydraulic conductivity at lower swelling pressures (densities) in material exposed to iron may be explained by ion exchange between sodium originally in the interlayer exchange positions and iron (II) released by corrosion. However, a change to divalent ions does not generally lead to changes in hydraulic conductivity at high swelling pressures (densities) /Karnland et al. 2005/. The results are rather typical of inhomogeneous systems with localised high density volumes and low density volumes /Börgesson et al. 2003/. In such systems, the high density volumes lead to higher swelling pressure and the low density volumes lead to higher hydraulic conductivity compared to a homogenous material. Speculatively, the results may consequently be explained by iron particles in the clay matrix leading to an inhomogeneous clay phase, or reduced homogenisation ability of the clay phase due to cementing iron compounds. However, the relatively low iron content and the microscopy data do not support the iron particle explanation. Similar results with high swelling pressure and increased hydraulic conductivity were found also in bentonite material exposed to corroding iron in laboratory tests performed to simulate the conditions in a KBS-3H repository /Börgesson et al. 2005/. These experiments were, however, not performed under oxygen-free conditions.

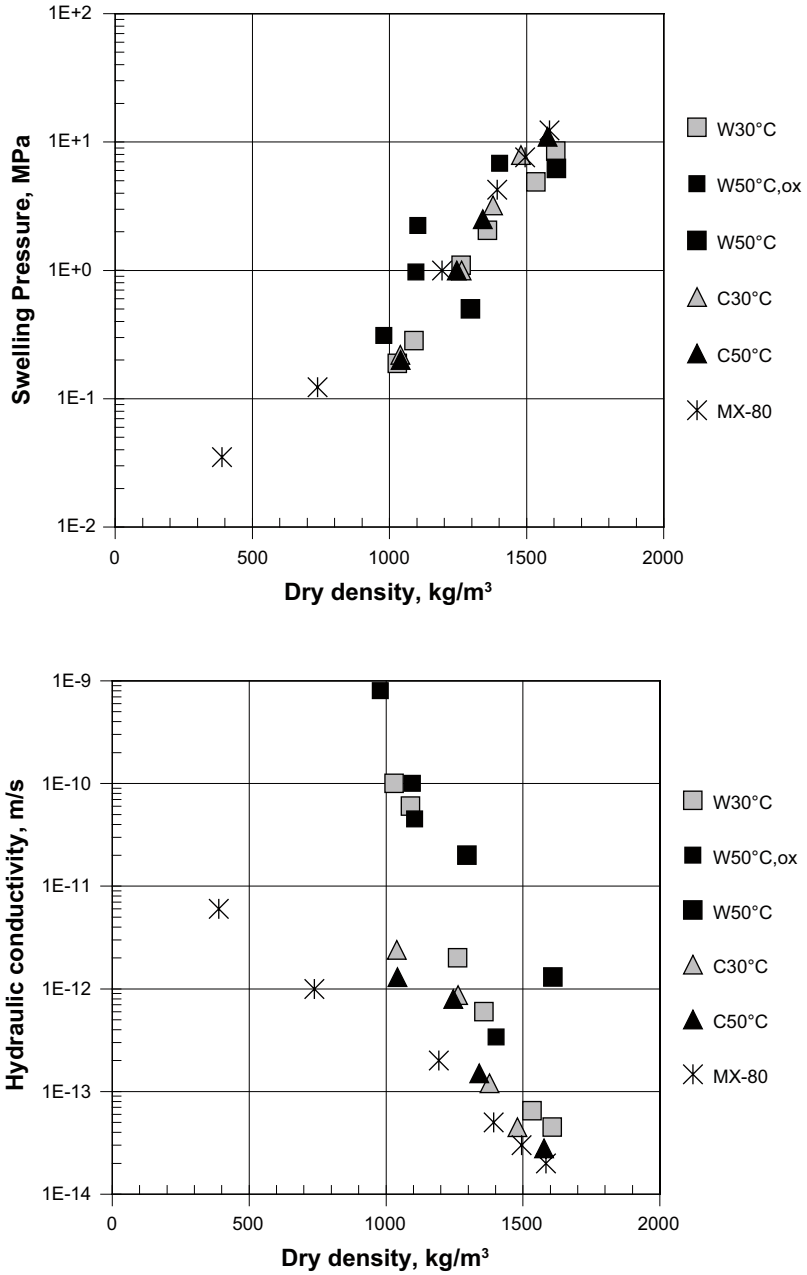

Figure 5-17. *Measured swelling pressure (upper) and hydraulic conductivity (lower) as a function of reduced clay dry density. C indicates coupon samples, W indicates wire samples, W50°C, ox indicates a slightly oxidized wire 50C material.*

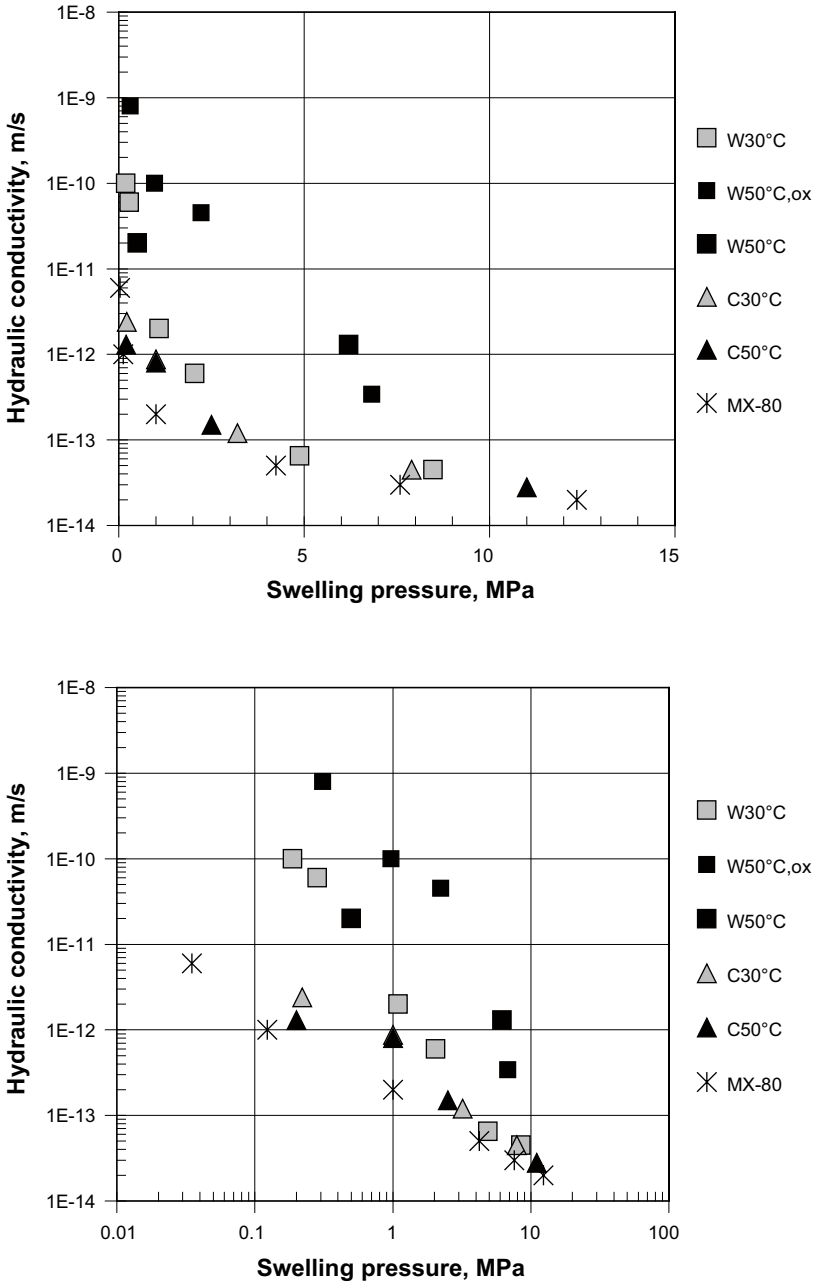

Figure 5-18. *Measured hydraulic conductivity versus measured swelling pressure. Linear pressure scale (upper) and logarithmic pressure scale (lower). C indicates coupon samples, W indicates wire samples, W50°C, ox indicates a slightly oxidized wire 50C material.*

6 Discussion and conclusions

6.1 Coupon tests

During the tests with cast iron and carbon steel coupons (356 days at 50°C and 900 days at 30°C), no major changes in the bentonite occurred. The colour of the bentonite was grey, as for fresh MX-80. A narrow zone with black and brown corrosion products could be seen where the bentonite had been in contact with metallic iron. According to SEM-EPMA mapping the zone affected by iron was 0.15 – 1.25 mm thick. Outside this zone the chemical composition of the bentonite was more or less the same as that of fresh MX80, apart for changes in the Ca and Na contents brought about by cation exchange with the background electrolyte. The oxide minerals magnetite, hematite and goethite could be identified using laser Raman spectroscopy on the surface of the coupons, although the higher oxidation state compounds may have been due to experimental artefacts. The XRD patterns of the coupon samples display a d_{001} spacing of 12.5 Å, which is typical of the one-layer hydration state of Na–montmorillonite. If significant amounts of iron had been incorporated in the montmorillonite interlayers, the d_{001}-spacing would be expected to be larger. However, the XRD data are inconclusive since there was no precise control of the relative humidity during the X-ray scanning. The Mössbauer analysis showed that the Fe^{2+}/Fe^{3+} ratio of the coupon samples was similar to that of fresh MX80 and according to the FTIR spectra, no changes occurred in the octahedral montmorillonite sheets of the coupon bentonites. The cation exchange capacity of the bentonite was essentially unchanged after the tests and exchange sites were saturated with the same cations as initially present in MX80, i.e. Na, K, Ca and Mg, although with an increased proportion of Na due to exchange with the Na-salt solution used in the tests.

6.2 Wire tests

Many more changes were observed in the tests with carbon steel wires in compacted bentonite (829 days at 30°C and 911 days at 50°C). This is to be expected because the surface area of metallic iron was much higher (111×) in the tests performed with pieces of wire than in those with coupons. The bentonite was strongly aggregated and had a blackish or bluish green colour characteristic of bentonite in reducing environments /Kamei et al. 1999/. The green colour can be explained by the reduction of Fe^{3+} in the octahedral montmorillonite sheets /Komadel et al. 1990/, by the presence of Fe(II) in the interlayer positions or by the presence of $Fe(OH)_2$ and Fe_3O_4 or a mixture of the two /Xia et al. 2004/.

The Mössbauer analysis confirmed that the major part of the iron, 74–78%, was present as ferrous iron, but indicated no significant quantities of iron oxides or oxyhydroxides. The iron was located in a chemical environment similar to that of the iron in MX-80, although not necessarily exactly the same. Similarly, FTIR spectra showed that bands involving octahedral Fe^{2+} were more intense in patterns of unoxidized wire bentonite and those involving Fe^{3+} were almost absent. When the bentonite was partially oxidized, the band involving Fe^{3+} increased in intensity and the band involving Fe^{2+} decreased in intensity. The change was paralleled by a change in the colour to olive green. The FTIR patterns of fully oxidised wire bentonite (brown) were identical to those of MX80, suggesting that some octahedral iron in the montmorillonite structure had been reduced during contact with corroding metallic iron.

The electron microprobe analysis and the chemical composition of the bentonite clearly showed that iron released from corroding wires had entered into the bentonite matrix. The concentration of iron was high, up to 20%, near corroding wires and decreased with increasing distance away

from the corroding surfaces. This suggests that the amount of iron entering into the bentonite matrix was determined by some kind of mass transport process away from the corroding surface. Laser Raman spectroscopy of the wire surface identified magnetite, but the layer of corrosion product was thin compared to what is normally observed on samples tested in aqueous conditions with no bentonite present. Raman spectroscopy of bentonite near the corroding wires did not identify any specific corrosion products. The lack of thick layers of corrosion products supports the view that iron released by corrosion entered into the bentonite rather than forming solid corrosion products.

As a consequence, the total iron content of the bentonite matrix had increased significantly – the amount of Fe in the wire bentonite samples corresponded to an addition of between 6.6 and 8.7% extra iron to MX80 (cf. Table 5-10). Since less than 3% Fe(II) is required to saturate all exchange sites in MX80, it is clear that iron had been incorporated far in excess of the cation exchange capacity of the starting material. And yet, a major portion of the exchange sites seemed to be occupied by a remnant cation pool dominated by Na and Ca.

The question is in what form all the additional iron had been incorporated. None of the techniques applied (X-ray diffraction and transmission electron diffraction analysis, Raman and Mössbauer spectroscopy) were able to detect any discrete neoformed iron-rich clay minerals (e.g. chlorite, berthierine) or corrosion products within the bentonite matrix. Apparently, higher temperatures than 50°C are required for such mineral transformations. Moreover, the rapid change in colour from green to brown of the wet bentonite when exposed to air suggested that iron must be in a form that allows rapid oxidation and oxide formation /Fialips et al. 2002/, i.e. either as $Fe(OH)_2$, another unstable compound, such as green rust, or as adsorbed iron.

One obvious effect of the incorporation of iron into the bentonite was a loss of cation exchange capacity. This suggests that iron was adsorbed onto exchange sites by a less reversible mechanism than regular cation exchange, possibly onto favoured sites on sheet surfaces or at mineral discontinuities in the montmorillonite. According to /Helsen and Goodman 1983/ and /Charlet and Tournassat 2005/ adsorption of Fe(II) onto clays in a non-exchangeable form will occur if pH is higher than 3–4.

A d(001) spacing in the range 14 to 15 Å has been reported for the reaction products obtained in anoxic experiments with Na-montmorillonite and aqueous solutions of Fe(II) /Wilson et al. 2000, Kozai et al. 2001/. No discrete 14 Å phase was detected in the reaction product of our experiments, in which Fe(II) was supplied by corrosion of metallic iron in a background electrolyte of sodium salts (0.55 M Na^+). Although a significant amount of non-exchangeable iron had been incorporated into the bentonite, thereby blocking some exchange sites, the remnant pool of exchangeable cations was still dominated by Na. Therefore, the composition of the interlayer material may have varied from one interlayer to another, giving a randomly interstratified structure. The available XRD data do no contradict such interpretation but are ambiguous due to poor control of the relative humidity during the X-ray scans.

Another effect of the incorporation of iron was a significant change in hydraulic conductivity of the bentonite, especially in the sample tested at 50°C. The increase in hydraulic conductivity at lower swelling pressure (densities) may be explained by the displacement of sodium by non-exchangeable iron. However, the results are also typical of inhomogeneous systems, in which localised high density volumes lead to higher swelling pressure and low density volumes lead to higher hydraulic conductivity compared to a homogenous material /Börgesson et al. 2003/. The results may consequently be explained by the presence of iron-rich particles or cementing iron compounds in the clay matrix leading to an inhomogeneous clay phase. The TEM-EDS analysis, showing that the concentration of iron within each montmorillonite grain/aggregate varied considerably, supports the view that part of the iron occurs as some kind of cement or surface coating.

The Indian bentonite Kutch 8939 used as control sample contained the iron oxides hematite and goethite. The total iron content (as FeO) is 8.8%, which is somewhat less than in the bentonites from the wire corrosion tests. Most of the iron is present as Fe^{3+}. Comparison of the mineralogical and chemical characteristics of the Indian bentonite with the bentonite from the wire tests is complicated due to the fact that Kutch 8939 was formed in an oxidizing environment whereas the conditions during the corrosion test were reducing.

The chemical location of Fe(II) in the wire bentonite samples is uncertain and the incorporation may be a result of several mechanisms. In relation to the use of bentonite as a buffer material for radioactive waste disposal, the incorporation of iron into bentonite at concentration levels of 7–8% leads to lower cation exchange capacity and a higher hydraulic conductivity, at the buffer densities expected in the near-field of a spent fuel repository.

7 Summary

Two types of corrosion tests were performed in a background electrolyte of sodium salts, one with cast iron and carbon steel coupons (mass 5.5 g, total surface area 0.0009 m^2) and one with carbon steel wires (mass 75 g, total surface area 0.1 m^2), both at two temperatures, 30°C and 50°C.

No major changes were observed in the bentonite after the tests with cast iron and carbon steel coupons. In the tests with carbon steel wires, an incorporation of iron into bentonite at concentration levels of 7–8% resulted in lower cation exchange capacity and a higher hydraulic conductivity. Four possible types of chemical/mineralogical changes brought about by the presence of metallic iron in contact with compacted bentonite in anaerobic conditions can be considered:

1) **Substitution of interlayer Na by iron/iron complexes in montmorillonite.** Fe^{2+} released from corroding carbon steel and cast iron into the pore water potentially brings about cation exchange. If iron had replaced the interlayer cations of MX80, the d_{001}-spacing would be expected to increase from ca 12.5 Å to ca 14–15 Å, but no discrete 14 Å phase was detected. However, the exchangeable cation data show that the pool of exchangeable cations was still dominated by Na, although iron had been incorporated far in excess of the cation exchange capacity of the starting material. The cation exchange capacity was reduced because non-exchangeable iron blocked some exchange sites. Hypothetically, specific adsorption of iron onto favoured sites on sheet surfaces in the montmorillonite may have resulted in a randomly mixed-layered structure. The available XRD data do no contradict such interpretation but are ambiguous since there was no precise control of the relative humidity during the X-ray scanning.

2) **Formation of magnetite or $Fe(OH)_2$ by precipitation of Fe^{2+} dissolved in pore water.** It is obvious from the TEM-EDS analysis and total chemical analysis that additional iron was present in both wire bentonite samples, giving local iron concentrations as high as 20%. The Fe content of single montmorillonite grains/aggregates varied considerably, suggesting that iron occurred as some kind of cement or surface coating, and this would certainly affect the physical properties of the bentonite. On the other hand, no iron oxide minerals could be detected with XRD, TEM, FTIR or Mössbauer spectroscopy. $Fe(OH)_2$ is very unstable, transforming easily to magnetite, and it is improbable that it could survive until identified. Magnetite is relatively stable but its identification with XRD is difficult unless the mineral is well ordered and there is a sufficient amount of it in the sample. Iron causes scattering of X-rays that raises the background level and reduces the peak intensities.

3) **Reduction of octahedral Fe^{3+} in montmorillonite brought about by the presence of a strong reducer, metallic iron.** Fe^{2+} instead of Fe^{3+} in octahedral montmorillonite sheets would increase the negative layer charge and change many properties of bentonite (e.g. increase cation exchange capacity). On the other hand, it has been noticed that the reduction of iron in montmorillonite leads to a decrease in specific surface area, probably because of Na-fixation and collapse of expandable layers /Lear and Stucki 1989/. According to FTIR spectra, Fe^{3+} in both wire bentonites was partly reduced to Fe^{2+}. Mössbauer spectra prove that Fe^{2+} was the dominating form of iron in both wire bentonites. If reduction of Fe^{3+} in the montmorillonite structure was followed by a collapse of some interlayers due to Na-fixation, the exchange capacity would decrease and the swelling properties would be changed.

4) **Formation of Fe-rich clay mineral phases** that involves major changes in the clay mineral structure. There was no indication that iron produced by the low temperature anaerobic corrosion of steel caused a transformation of montmorillonite to a different iron-rich mineral phase such as chlorite or berthierine, or resulted in build-up of Fe in the octahedral montmorillonite sheets. The only change recorded in the montmorillonite octahedral sheets is reduction of Fe^{3+} to Fe^{2+}.

References

Bishop J L, Murad E, 2004. Characterisation of minerals and biogeochemical markers on Mars: A Raman and IR spectroscopic study of montmorillonite, J. Raman Spectroscopy 35, 480–486.

Brindley G W, Brown G, 1980. Crystal structures of clay minerals and their X-ray identification. Mineralogical Society Mon. No. 5. 495 pp.

Börgesson L, Johannesson L-E, Gunnarsson D, 2003. Influence of soil structure heterogeneities on the behavior of backfill materials based on mixtures of bentonite and crushed rock. Applied Clay Science 23, 121–131.

Börgesson L, Sandén T, Fälth B, Åkesson M, Lindgren E, 2005. Behavior of the buffer in KBS-3H. SKB R-05-50, Svensk Kärnbränslehantering AB.

Carlson L, 2004. Bentonite mineralogy. Part 1: Methods of investigation – a literature review. Part 2: Mineralogical research of selected bentonites. Posiva WR 2004-02.

Charlet L, Tournassat C, 2005. Fe(II)-Na(I)-Ca(II) cation exchange on montmorillonite in chloride medium: evidence for preferential clay adsorption of chloride-metal ion pairs in seawater. Aquatic Geochemistry 11. 115–137.

Farmer V C (ed), 1974. The infrared spectra of clay minerals. Minerological Society, London.

Fialips C-I, Huo D, Yan L, Wu J, Stucki J W, 2002. Infrared study of reduced and reduced-reoxidized ferruginous smectite. Clays and Clay Minerals 50, 455–469.

Guillaume D, Neaman A, Cathelineau M, Mosser-Ruck R, Peiffert C, Abdemoula M, Dubessy J, Villieras F, Baronnet A, Michau N, 2003. Experimental synthesis of chlorite from smectite at 300°C in the presence of metallic Fe. Clay Minerals 38, 281–302.

Helsen J A, Goodman B A, 1983. Characterization of iron(II) and iron(III)-exchanged montmorillonite and hectorite using the Mössbauer effect. Clay Minerals 18, 117–125.

Idemitsu K, Yano S, Xia X, Kikuchi Y, Inagaki Y, Arima T, 2003. Migration behavior of iron in compacted bentonite under reducing condition by using electromigration. Materials Research Society Symposium Proceedings, 757, II3.7.1–II3.7.8.

Kamei G, Oda C, Mitsui S, Shibata M, Shinozaki T, 1999. Fe(II)-Na ion exchange at interlayers of smectite: adsorption-desorption experiments and a natural analogue. Engineering Geology 54, 15–20.

Karnland O, Olsson S, Nilsson U, Sellin P, 2005. Experimental study on the sealing properties of commercial bentonites related to bentonite mineralogy and water solution composition. Conference abstract ANDRA Tours 2nd International Conference 2005. 229.

Komadel P, Lear P R, Stucki J W, 1990. Reduction and reoxidation of nontronite: Extent of reduction and reaction rates. Clays and Clay Minerals 38, 203–208.

Komadel P, Madejova J, Stucki J, 1999. Partial stabilization of Fe(II) in reduced ferruginous smectite by Li fixation. Clays and Clay Minerals 47, 458–465.

Kostka J E, Wu J, Nealson K H, Stucki J, 1999. The impact of structural Fe(III) reduction by bacteria on the surface chemistry of smectite clay minerals. Geochimica et Cosmochimica Acta 63, 3705–3713.

Kozai N, Adachi Y, Kawamura S, Inada K, Kozaki T, Sato S, Ohashi H, Ohnuki T, Banba T, 2001. Characterization of Fe-montmorillonite: a simulant of buffer materials accommodating overpack corrosion product. J. of Nuclear Science and Technology 38. 1141–1143.

Lantenois S, 2003. Réactivité fer métal/smectites en milieu hydraté à 80°C. Ph.D. thesis, University of Orleans.

Lear P R, Stucki J W, 1989. Effects of iron oxidation state on the specific surface area of nontronite. Clays and Clay Minerals 37, 547–552.

Manceau A, Drits V A, Lanson B, Chateigner D, Wu J, Huo D, Gates W P, Stucki J W, 2000. Oxidation-reduction mechanism of iron in dioctahedral smectites: II. Crystal chemistry of reduced Garfield nontronite. American Mineralogist 85, 153–172.

Meier L P, Kahr G, 1999. Determination of the cation exchange capacity (CEC) of clay minerals using the complexes of copper(II) ion with triethylenetetraamine and tetraethylenepentamine. Clays and Clay Minerals 47, 386–388.

Smart N R, Rance A P, Werme L, 2004. Anaerobic corrosion of steel in bentonite. Materials Research Society Symposium Proceedings 807, 441–446.

Stucki J W, Low P F, Roth C B, Golden D C, 1984. Effects of oxidation state of octahedral iron on clay swelling. Clays and Clay Minerals 32, 357–362.

Vértes A, Czakó-Nagy I, 1989. Mössbauer spectroscopy and its application to corrosion studies, Electrochimica Acta 34(6), 721–758.

Vicente M A, Suarez M, Bañares-Muñoz M A, Pozas J M M, 1998. Reduction of Fe(III) in a high-iron saponite. Pillaring of the reduced samples with Al_{13} polymers. Clay Minerals 33, 213–220.

Wilson J, Ragnarsdottir V, Savage D, Cressey G, 2000. The effect of iron on the stability of montmorillonite. Goldschmidt 2000. Journal Conference Abstracts, vol. 5(2) 1097.

Wilson J, Cressey G, Cressey B, Cuadros J, Ragnarsdottir K V, Savage D, Shibata M, 2005. The effect of iron reactions between native Fe, magnetite, montmorillonite and aqueous solutions: (II) experimental investigation. (Submitted to Geochimica et Cosmochimica Acta).

Xia X, Idemitsu K, Arima T, Inagaki Y, Ishidera T, Kurosawa S, Iijima K, Sato H, 2004. Corrosion of carbon steel in compacted bentonite and its effect on neptunium diffusion under reducing conditions. Applied Clay Science, 89–100.

Appendix 1

Visual appearance

Sample	Appearance and texture
Compacted bentonite, 30°C, wires	Block of bentonite was very dark. Bentonite matrix was crumbly and wires fell out easily. Wires appeared dark but quite clean, without a thick black layer. Bentonite at the base of the block was light brown – could be due to drying (Figure A1-1).
Compacted bentonite, 50°C, wires	Block of bentonite was very dark with light brown regions at the edge; central region was black. Bentonite matrix was crumbly with a slight brown-green tinge when powdered. Wires fell out easily. They appeared quite clean, without a thick black layer (Figure A1-2).
Compacted bentonite, 30°C, coupons	Bentonite block cracked after drying. Area in direct contact with cast iron was black or dark grey (Figure A1-3) with a light brown layer surrounding the coupon, approximately 2–2.5 mm deep into the bentonite. Cast iron specimen dull grey. Coupons did not have a thick layer of oxide. Samples for analysis included both the black and light brown layers.
Compacted bentonite, 50°C, coupons	Cast iron black. Light brown layer surrounding coupons, approximately 2–2.5 mm deep (Figure A1-4). The bentonite at a distance from the coupon was light grey. Samples for analysis included both the black and light brown layers.

Figure A1-1. *Compacted bentonite, 30°C, wires. The specimen crumbled when a slice was removed from the end of the bentonite block.*

Figure A1-2. *Compacted bentonite, 50°C, wires. The specimen crumbled when a slice was removed from the end of the bentonite block.*

Figure A1-3. *Compacted bentonite, 30°C, coupons – top: location of cast iron coupon; bottom: location of carbon steel. Samples for XRD anoxic, Raman, SEM, Mössbauer analyses were taken from the centre of the black region. For XRD oxic, FTIR, TEM, CEC and total chemical analyses samples were taken from the grey bentonite and the black zone was removed.*

Figure A1-4. *Compacted bentonite, 50°C, coupons – location of cast iron coupon. Samples for XRD anoxic, Raman, SEM, Mössbauer analyses were taken from the centre of the black region. For XRD oxic, FTIR, TEM, CEC and total chemical analyses samples were taken from the grey bentonite and the black zone was removed.*

Appendix 2

XRD patterns (anoxic)

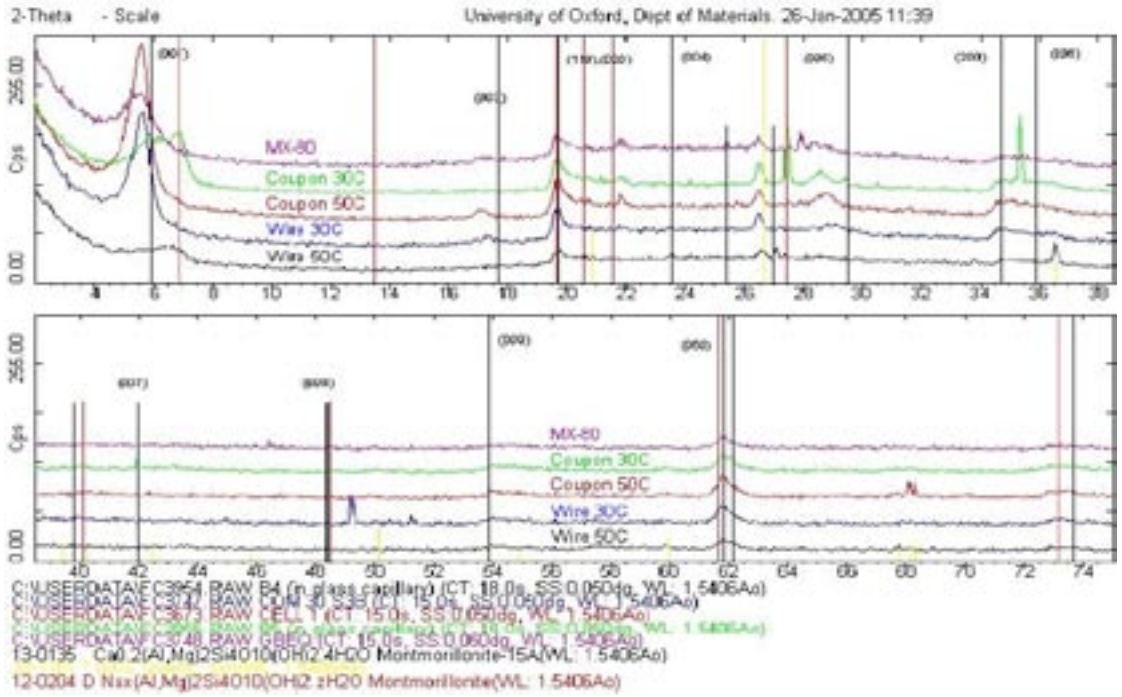

Figure A2-1. *Anoxic XRD patterns of MX-80 and the four bentonites from corrosion tests. The vertical lines indicate peak positions and intensities of standard montmorillonites (black – 15 Å; brown – 12 Å) and quartz (yellow). The numbers in parentheses indicate the Miller indices of montmorillonite peaks. All patterns are presented separately in following figures (A2-2 to A2-6).*

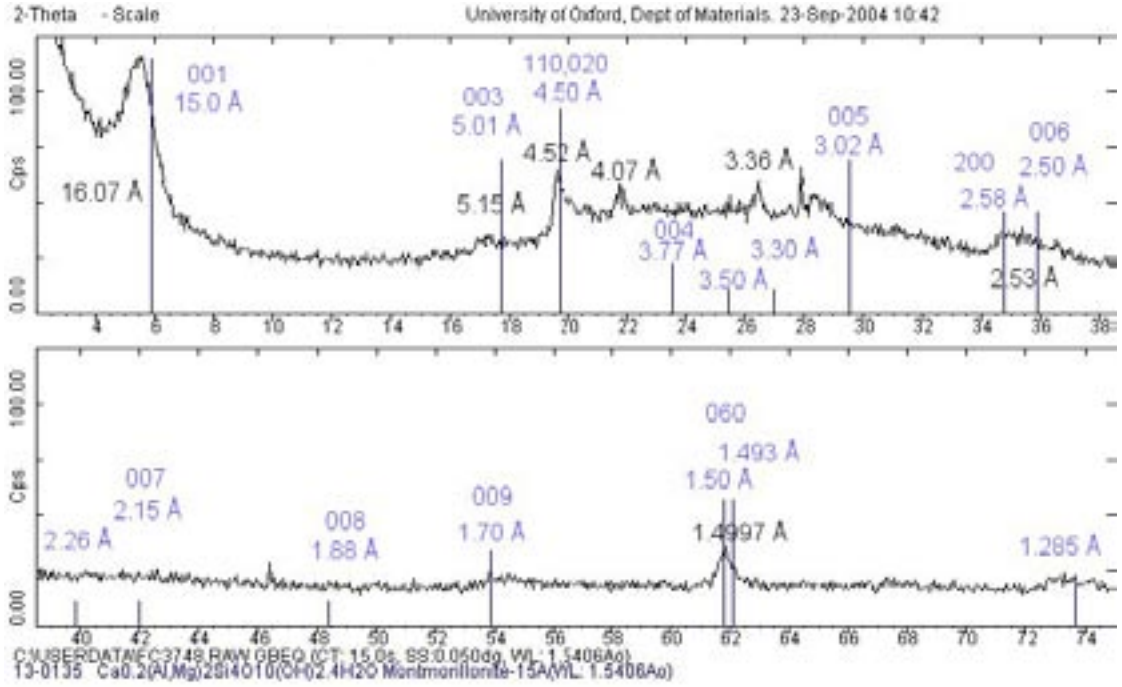

Figure A2-2. *XRD pattern of MX-80 equilibrated in glove box and packed in a glass capillary. The blue lines and figures indicate the peak positions, their d-values and Miller indices of standard Mg-exchanged montmorillonite. The black figures indicate d-values of peaks observed in the pattern. Relative humidity (RH) was apparently high. At RH 20–60% d_{001} of Na-montmorillonite is ca 12.5 Å.*

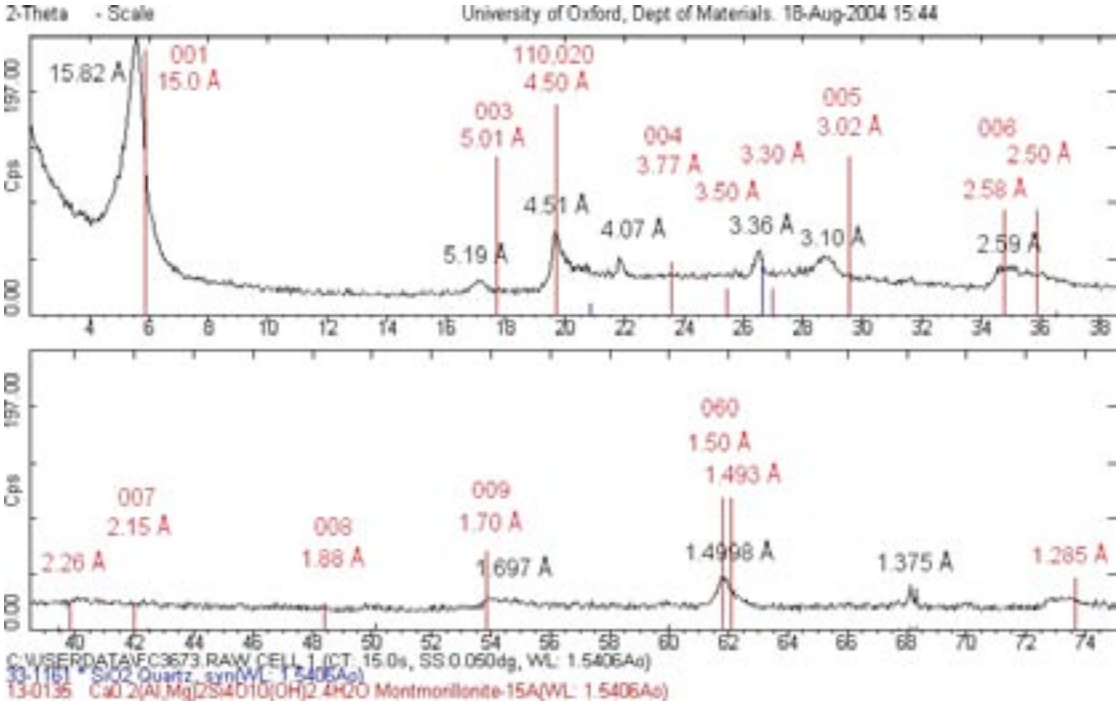

Figure A2-3. *XRD pattern of the coupon 50C bentonite equilibrated in glove box and packed in a glass capillary. The red lines and figures indicate the peak positions, their d-values and Miller indices of standard Mg-exchanged montmorillonite. The black figures indicate the d-values of peaks observed in the pattern.*

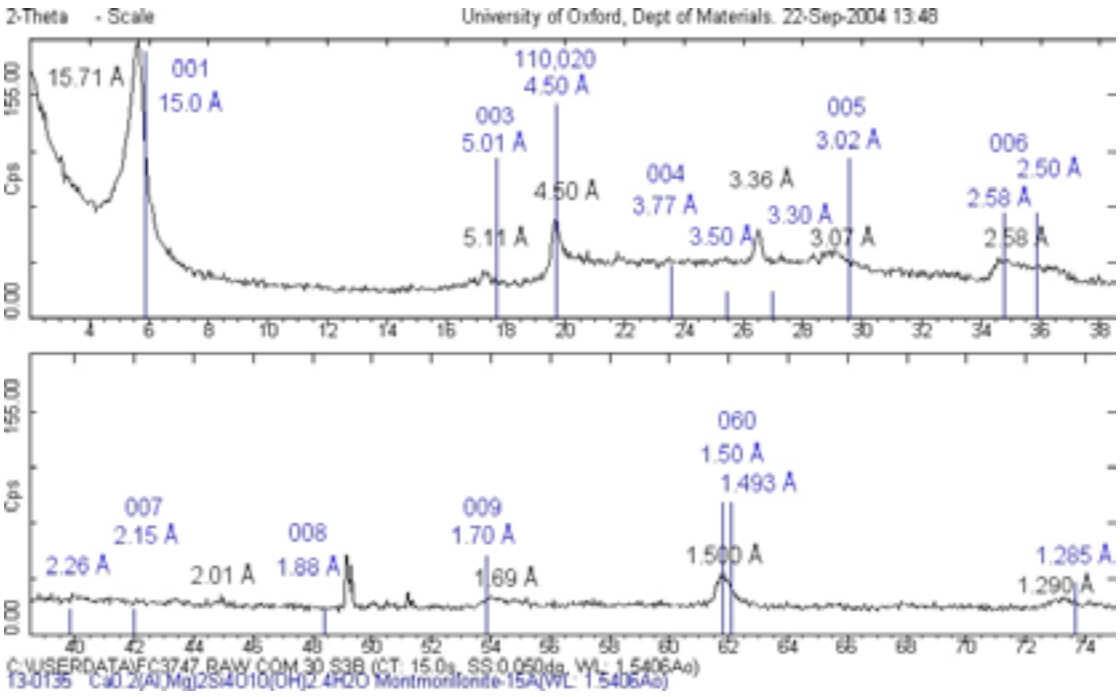

Figure A2-4. *XRD pattern of the wire 30C bentonite equilibrated in glove box and packed in a glass capillary. The blue lines and figures indicate the peak positions, their d-values and Miller indices of standard Mg-exchanged montmorillonite. The black figures indicate the d-values of peaks observed in the pattern.*

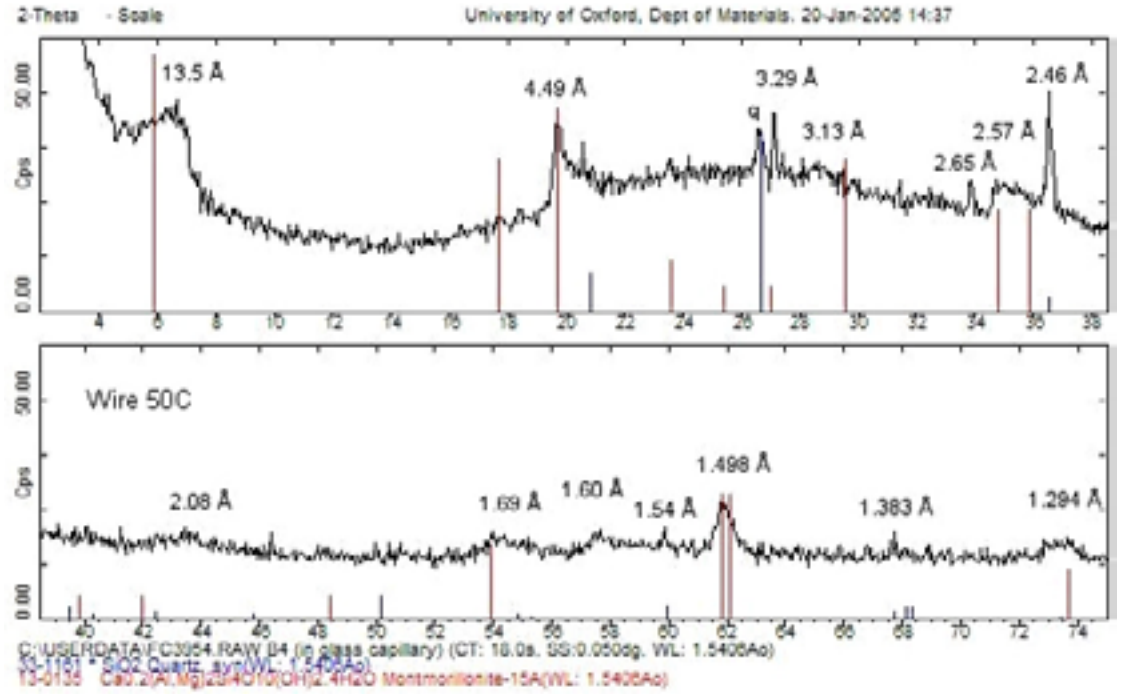

Figure A2-5. *XRD pattern of the wire 50C bentonite equilibrated in glove box and packed in a glass capillary at RH 14%. The red lines indicate the peak positions of a standard Mg-exchanged montmorillonite. The black figures indicate the d-values of peaks observed in the pattern. q, quartz. The sharp peaks at 3.29 and 2.46 Å are due to contamination of the glass capillary.*

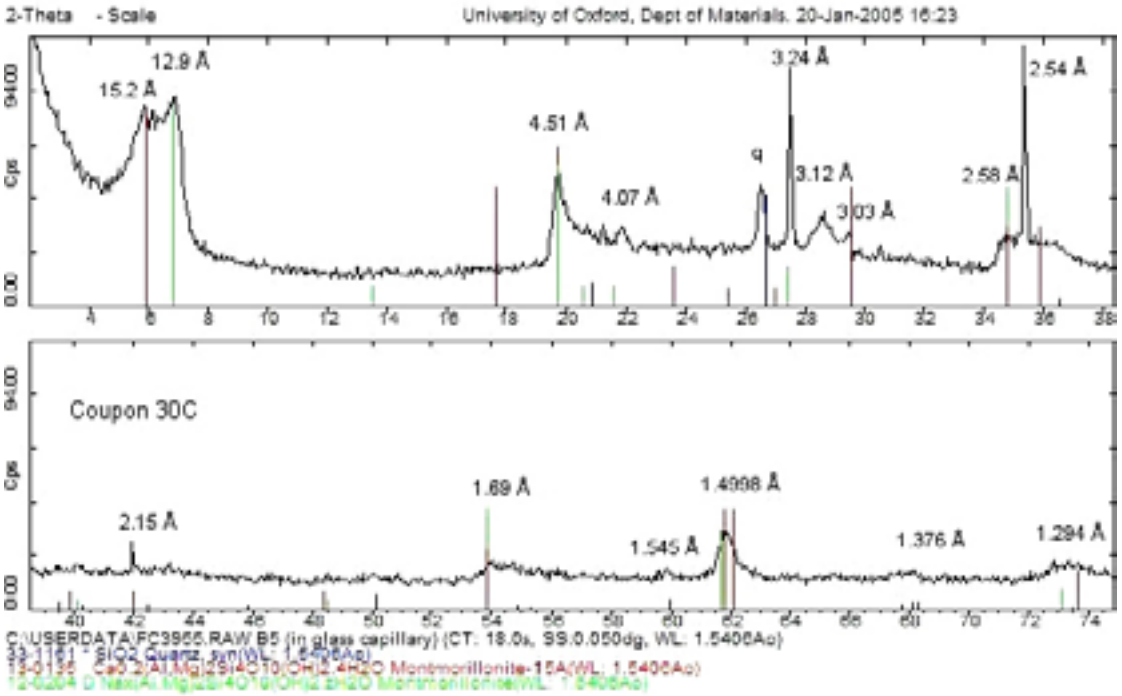

Figure A2-6. *XRD pattern of the coupon 30C bentonite equilibrated in glove box and packed in a glass capillary at RH 14%. The red and green lines indicate the peak positions of standard montmorillonites, the red with divalent interlayer cations (15 Å) and the green with Na as interlayer cation (12 Å). The black figures indicate the d-values of peaks observed in the pattern. q, quartz. The sharp peaks with d-values 3.24, 2.54 and 2.15 Å are due to contamination of the glass capillary.*

Appendix 3

SEM-EDX

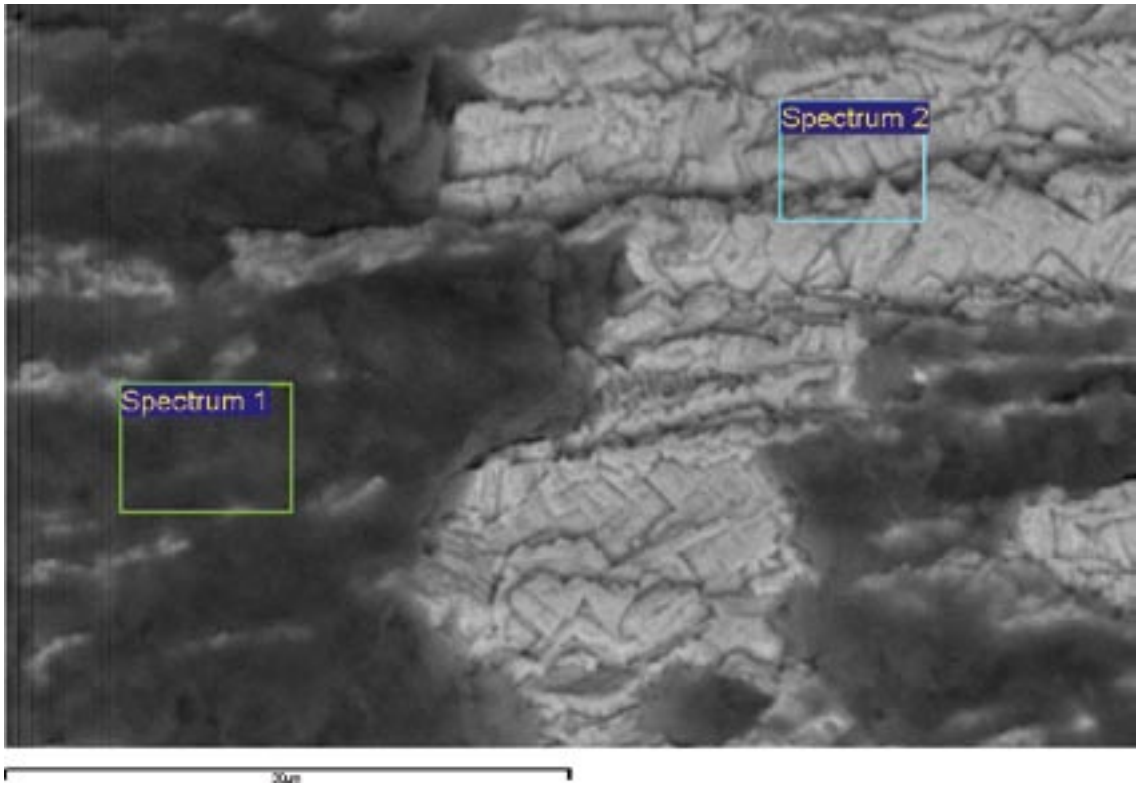

Spectrum	O	Na	Mg	Al	Si	S	Cl	Fe	Total
1	43.34	0.93	1.06	5.77	15.99		0.30	32.61	100
2					0.64	0.31		99.06	100

Figure A3-1. *Back scattered image of bentonite adhering to the surface of wire (829 days, 30°C). EDX analyses from two points in wt%. Bar, 30 µm.*

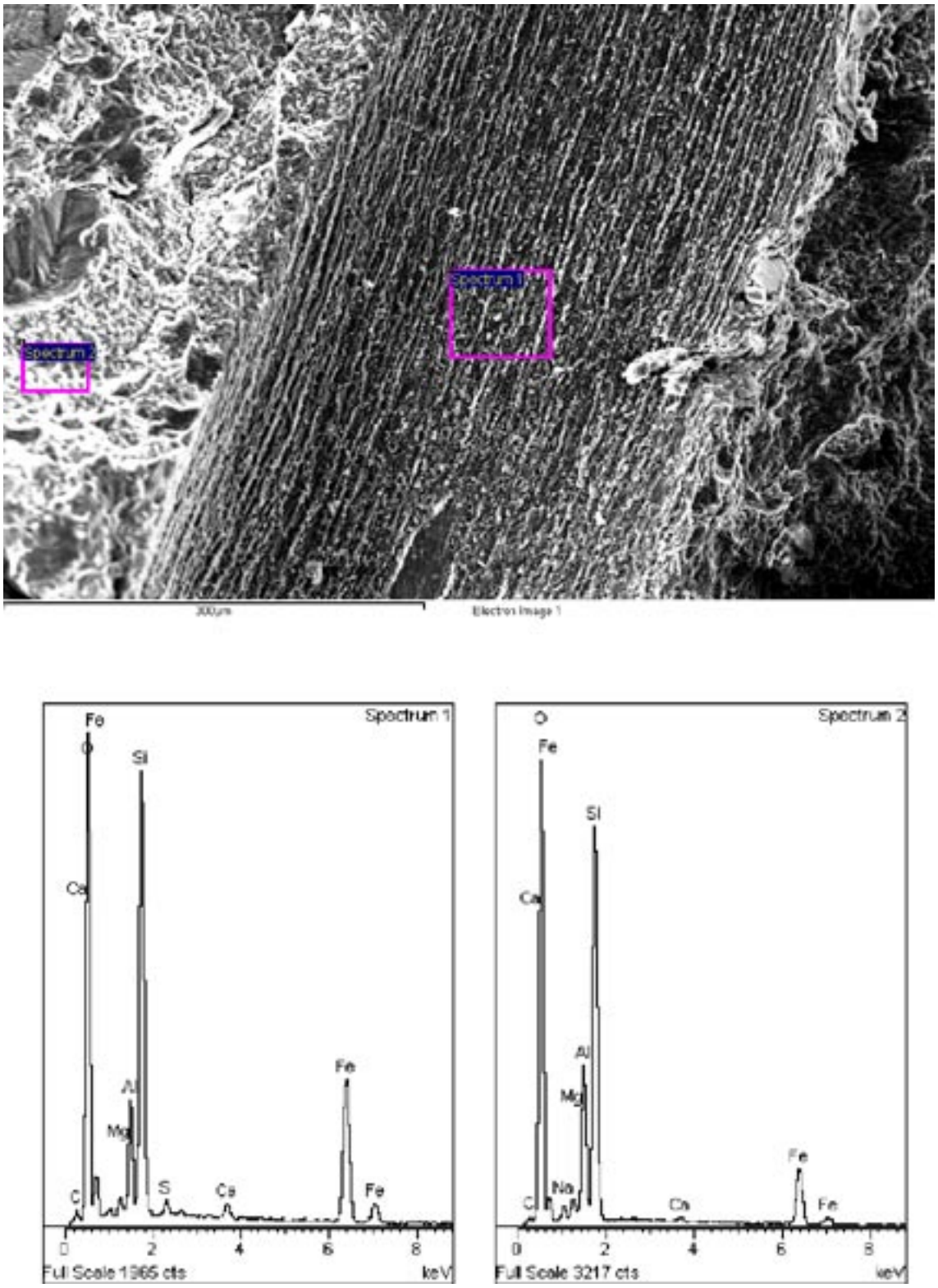

Figure A3-2. *SEM image of bentonite surface after removing a piece of wire (911 days at 50°C) and EDX spectra from two points. Bar, 300 µm.*

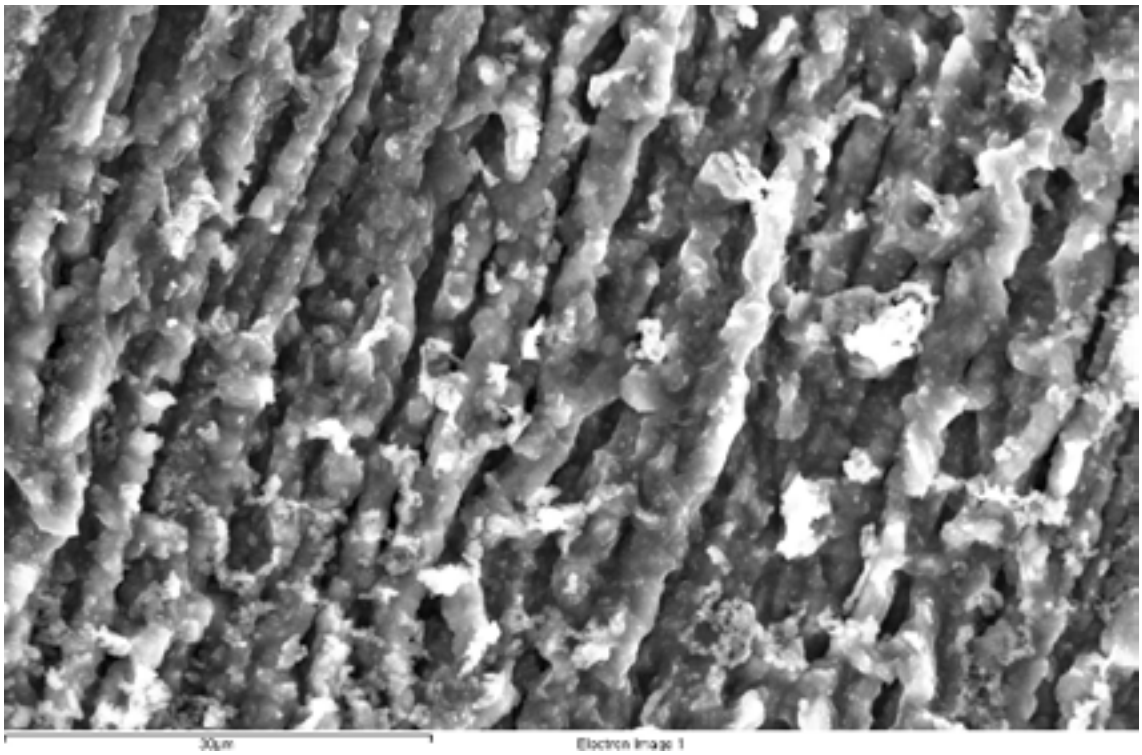

Figure A3-3. *A close-up of the bentonite surface in contact with a piece of wire (911 days at 50°C). Bar, 30 µm.*

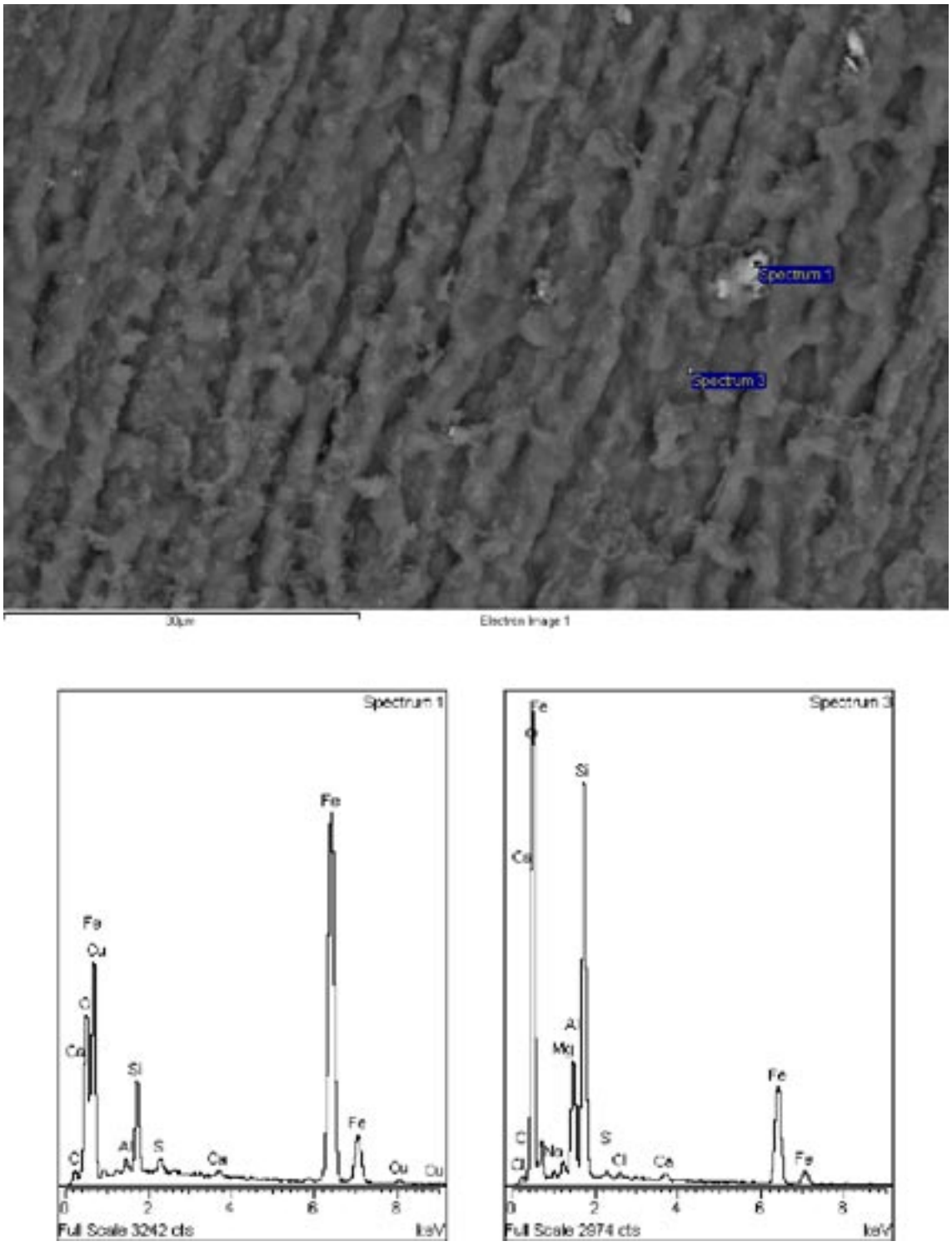

Figure A3-4. *Back scattered image of the bentonite surface in Figure A3-3. EDX spectra in two points as wt%. Bar, 30 µm.*

SEM-EPMA

a

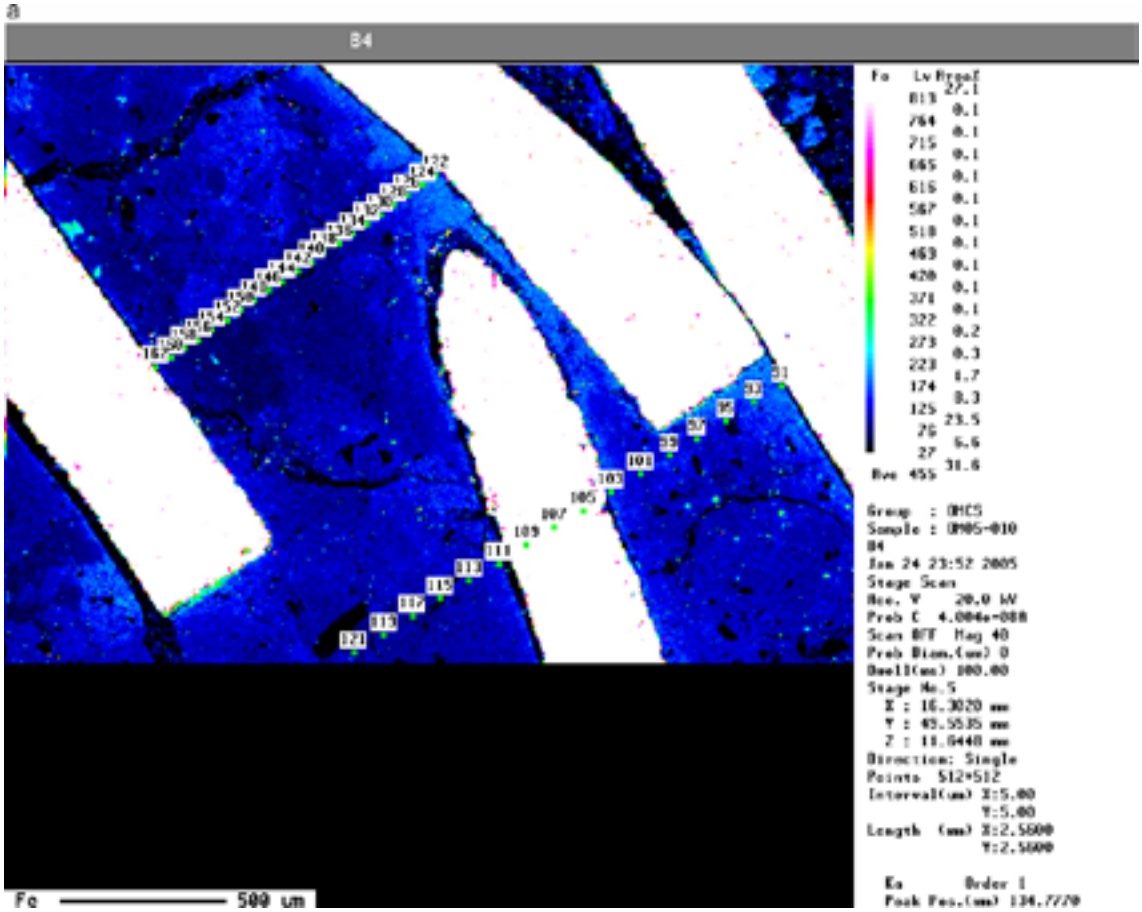
B4
Fe
500 um

b

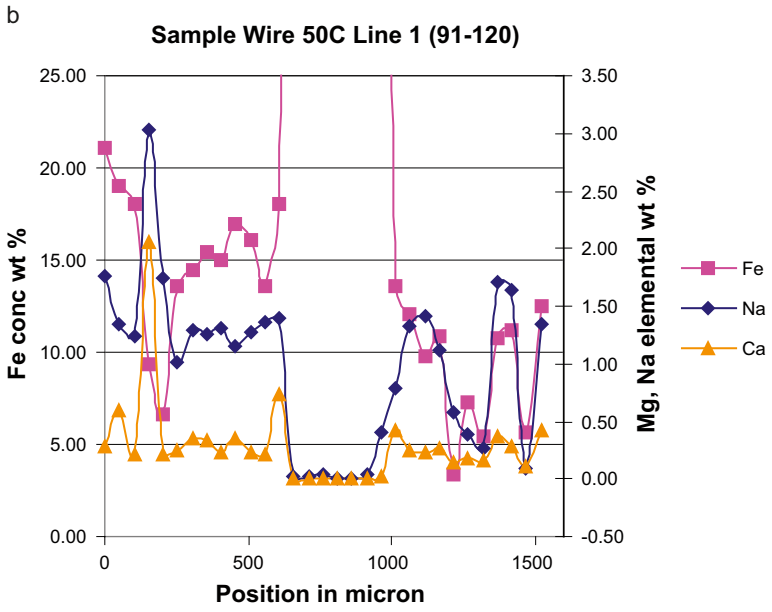
Sample Wire 50C Line 1 (91-120)
Fe conc wt %
Mg, Na elemental wt %
Position in micron
Fe
Na
Ca
25.00
20.00
15.00
10.00
5.00
0.00
3.50
3.00
2.50
2.00
1.50
1.00
0.50
0.00
-0.50
0
500
1000
1500

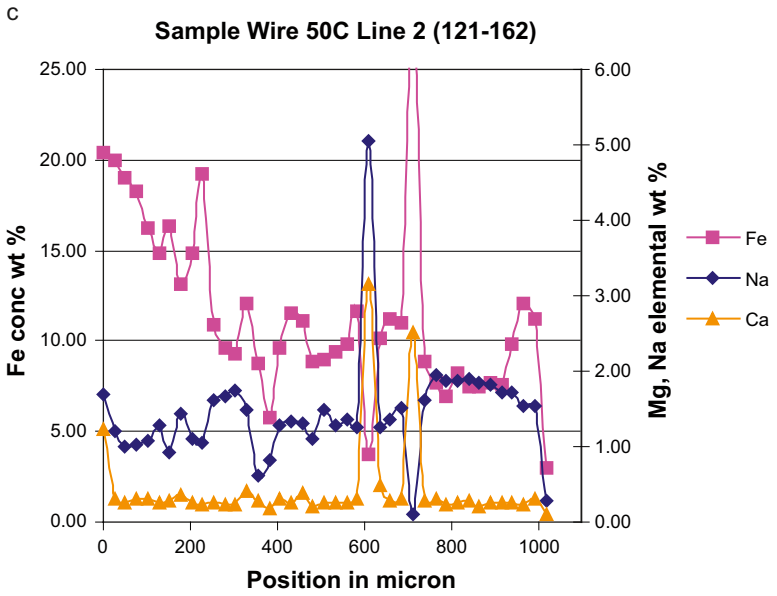

Figure A4-1. *SEM-EPMA map of compacted bentonite in contact with carbon steel wire for 911 days at 50°C (1a) and line plots of the concentrations of Fe, Na and Ca across the two lines (1b, 1c) given in Figure A4-1a. More detailed data on line 2 is given in Table A4-1.*

Table A4-1. SEM-EPMA point analyses (in wt%) of the bentonite in contact with carbon steel wire at 50°C. The location of point analyses are marked in Figure A4-1a, line 2.

No.	Na	Mg	Al	Si	S	Cl	K	Ca	Fe
122	1.68	1.02	6.49	21.24	0.03	0.07	0.26	1.22	20.43
124	1.00	1.15	8.94	20.22	0.00	0.02	0.08	0.25	19.04
126	1.08	1.25	10.18	22.03	0.01	0.02	0.13	0.31	16.24
128	0.92	1.06	8.87	19.71	0.00	0.01	0.07	0.27	16.31
130	1.09	1.29	10.06	22.10	0.01	0.02	0.08	0.26	14.83
132	1.62	1.33	11.39	24.35	0.01	0.02	0.15	0.26	10.87
134	1.75	0.92	10.99	24.72	0.01	0.05	2.16	0.22	9.31
136	0.62	0.59	5.71	13.29	0.01	0.11	0.14	0.27	8.78
138	1.28	1.07	9.44	21.60	0.02	0.16	0.12	0.30	9.65
140	1.31	0.99	9.32	20.77	0.03	0.18	0.90	0.39	11.10
142	1.48	1.13	10.73	22.80	0.00	0.07	0.10	0.25	9.01
144	1.36	1.16	10.86	23.40	0.01	0.07	0.08	0.26	9.82
146	5.06	0.24	12.70	27.85	0.02	0.09	0.67	3.14	3.75
148	1.36	1.24	10.22	23.67	0.01	0.06	0.32	0.28	11.20
150	0.10	4.65	0.48	0.89	0.01	0.04	0.01	2.51	28.74
152	1.94	2.02	11.42	25.41	0.01	0.03	0.15	0.31	7.73
154	1.88	1.98	10.82	24.87	0.00	0.02	0.13	0.26	8.19
156	1.84	1.92	10.92	25.11	0.00	0.02	0.15	0.22	7.49
158	1.72	1.86	10.65	24.67	0.00	0.04	0.16	0.25	7.63
160	1.54	1.65	9.48	22.95	0.38	0.05	0.23	0.24	12.07
162	0.27	0.30	1.50	3.86	0.05	0.25	0.01	0.10	3.04

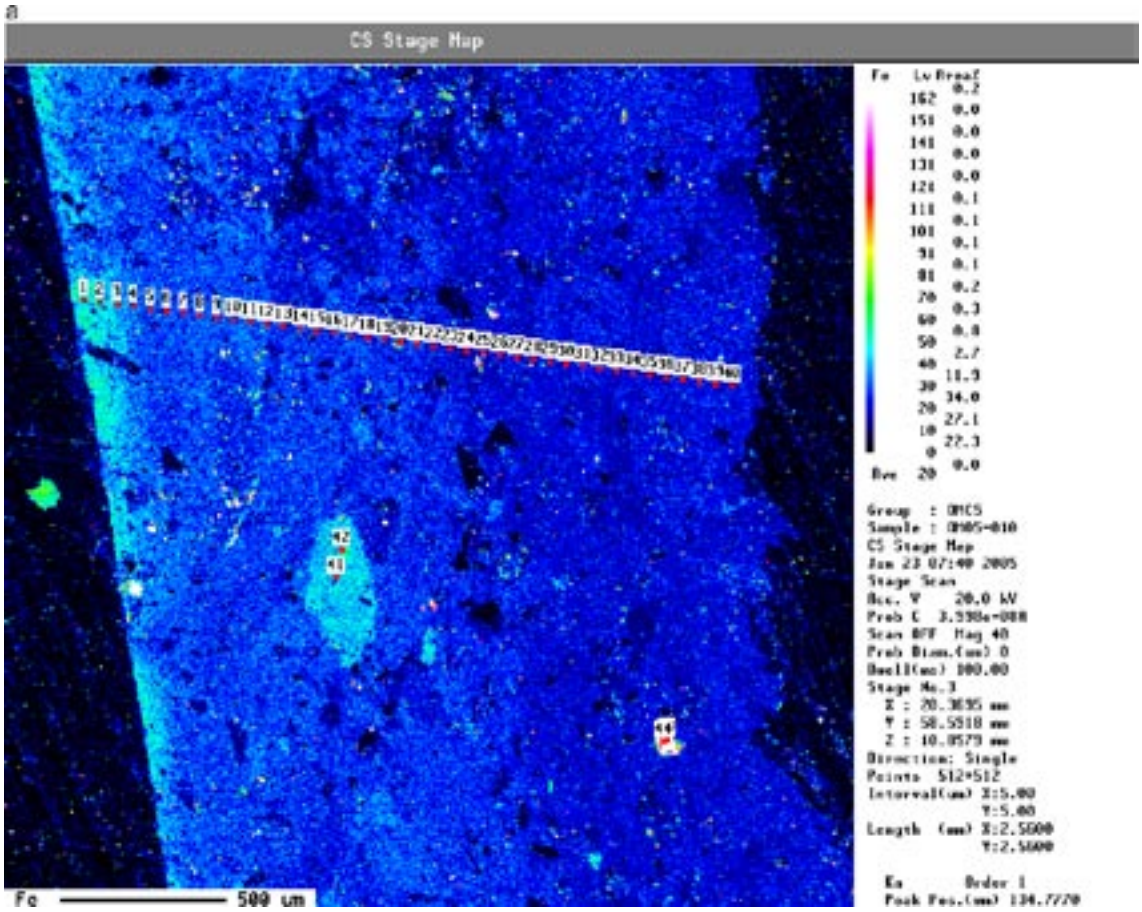

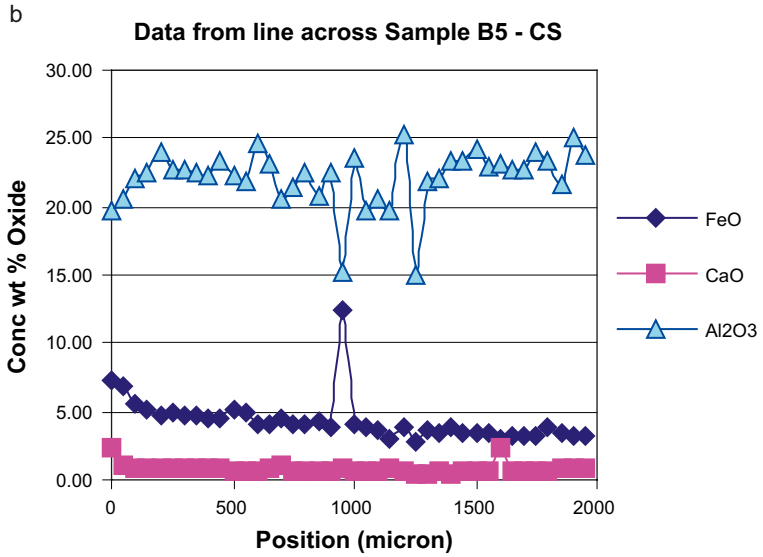

Figure A4-2. *EPMA map of the distribution of Fe in compacted bentonite in contact with a carbon steel coupon for 900 days at 30°C (2a). The sites of point analyses are marked. Line plots of the concentrations of FeO, CaO and Al_2O_3 (2b) across the line marked in Figure A4-2b. More detailed data are given in Table A4-2 (below).*

Table A4-2. SEM-EPMA point analyses (in wt%) of the bentonite in contact with carbon steel coupon at 30°C. The location of point analyses are marked in Figure A4-2a.

No.	Na_2O	MgO	Al_2O_3	SiO_2	SO_3	K_2O	CaO	MnO	FeO	Total
1	1.65	2.93	19.72	58.55	0.04	0.14	2.32	0.01	7.38	92.74
2	0.95	2.65	20.67	60.59	0.03	0.09	1.06	0.00	6.84	92.87
3	1.02	2.43	22.00	58.87	0.02	0.10	0.81	0.02	5.59	90.86
4	0.43	2.39	22.44	58.45	0.01	0.10	0.82	0.02	5.23	89.89
5	0.56	2.30	23.90	59.61	0.12	0.11	0.85	0.02	4.64	92.12
6	0.71	2.29	22.71	57.91	0.33	0.10	0.88	0.00	4.90	89.82
7	0.48	2.59	22.82	60.14	0.02	0.11	0.92	0.00	4.76	91.84
8	2.39	2.44	22.60	59.78	0.00	0.16	0.90	0.02	4.82	93.11
9	2.32	2.34	22.18	60.16	0.04	0.13	0.82	0.03	4.58	92.61
10	2.49	2.43	23.43	59.98	0.01	0.08	0.79	0.00	4.50	93.71
11	2.49	2.50	22.27	60.20	0.02	0.08	0.71	0.00	5.14	93.40
12	2.37	2.53	21.77	58.43	0.04	0.13	0.75	0.00	4.90	90.91
13	2.84	2.68	24.59	60.04	0.01	0.07	0.65	0.00	4.15	95.04
14	2.59	2.56	23.08	61.09	0.32	0.13	0.90	0.00	4.13	94.80
15	2.17	2.34	20.52	57.85	0.06	0.30	1.06	0.02	4.43	88.75
16	2.39	2.37	21.35	57.72	0.03	0.22	0.65	0.00	4.00	88.73
17	2.39	2.59	22.47	61.61	0.02	0.12	0.74	0.03	4.02	93.98
18	2.17	2.38	20.84	59.24	0.22	0.15	0.71	0.00	4.33	90.04
19	2.52	2.82	22.59	62.04	0.04	0.18	0.72	0.00	3.93	94.83
20	2.14	2.00	15.16	41.60	0.06	0.06	0.91	0.06	12.47	74.45
21	2.73	2.87	23.53	62.53	0.01	0.06	0.63	0.00	4.06	96.42
22	2.19	2.49	19.63	61.61	0.09	0.23	0.70	0.03	3.79	90.76
23	2.08	2.51	20.66	63.45	0.02	0.16	0.71	0.00	3.60	93.18
24	1.98	2.35	19.73	64.46	0.03	0.15	0.85	0.01	2.96	92.52
25	2.76	2.54	25.25	60.33	1.68	0.08	0.58	0.00	3.81	97.03
26	1.40	1.67	15.03	52.42	0.06	0.23	0.48	0.02	2.82	74.13
27	1.92	2.57	21.79	61.21	0.01	0.17	0.52	0.00	3.56	91.75
28	2.45	2.02	22.10	62.00	0.02	2.24	0.64	0.00	3.36	94.83
29	2.33	2.45	23.46	61.49	0.01	0.15	0.50	0.02	3.84	94.25
30	2.32	2.71	23.41	62.14	0.00	0.16	0.55	0.01	3.42	94.72
31	2.16	2.68	24.30	62.46	0.00	0.12	0.60	0.00	3.46	95.79
32	1.96	2.59	23.02	59.99	0.02	0.16	0.68	0.01	3.49	91.91
33	2.08	2.42	23.22	59.30	0.02	0.20	2.35	0.02	3.03	92.63
34	2.21	2.72	22.74	61.11	0.01	0.15	0.66	0.01	3.26	92.86
35	2.22	2.76	22.74	62.42	0.03	0.17	0.70	0.00	3.28	94.32
36	2.30	2.75	23.96	64.35	0.02	0.14	0.66	0.00	3.16	97.34
37	2.35	2.78	23.36	61.71	0.02	0.08	0.64	0.04	3.76	94.75
38	2.17	2.62	21.55	61.47	0.00	0.08	0.95	0.02	3.36	92.23
39	2.16	2.46	25.08	61.90	0.01	0.12	0.91	0.00	3.12	95.77
40	2.29	2.66	23.83	61.37	0.01	0.14	0.90	0.00	3.24	94.44
41	2.38	2.03	19.99	62.87	0.06	2.79	0.61	0.00	5.38	96.10
42	2.38	2.50	20.62	58.64	0.05	0.07	0.88	0.00	8.37	93.50
43	0.53	9.37	2.21	5.25	0.03	0.09	5.69	0.47	39.65	63.27
44	0.34	9.20	0.95	3.01	0.02	0.10	4.58	0.20	42.22	60.62

a

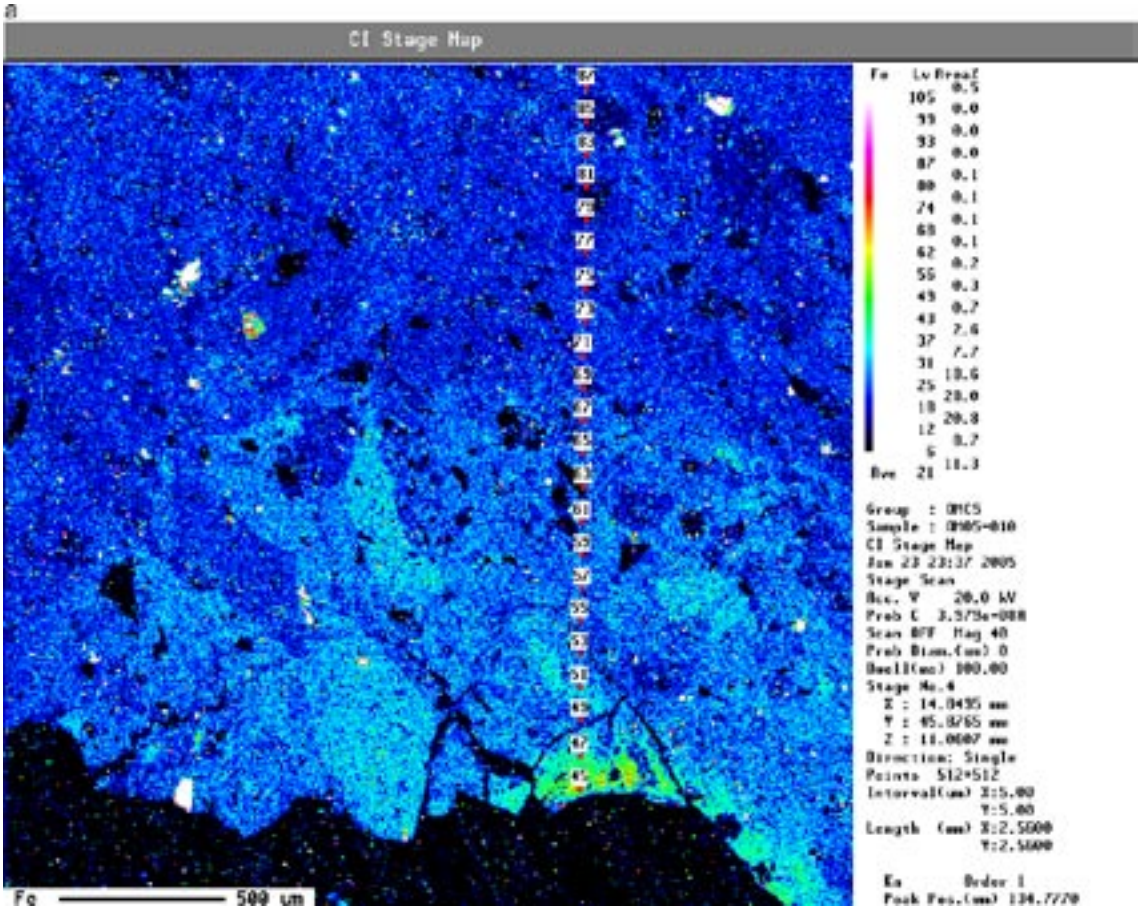

b

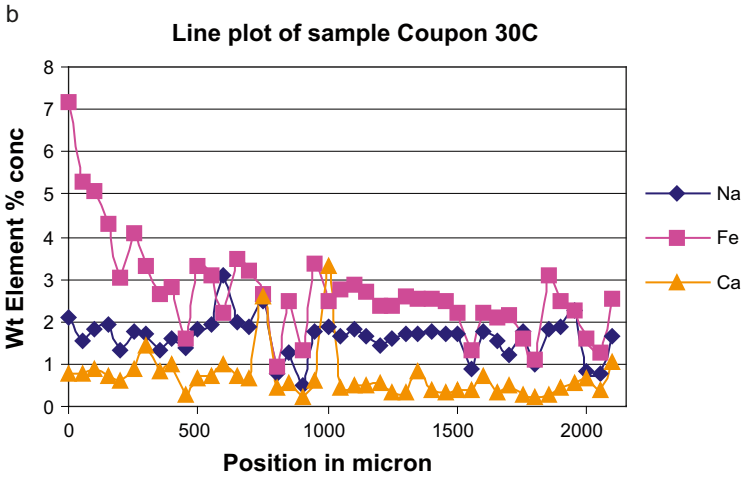

Figure A4-3. *EPMA map of the distribution of Fe in the compacted bentonite in contact with a cast iron coupon for 900 days at 30°C (3a) and line plots of the concentrations of Na, Fe and Ca (3b). The sites of point analyses are marked in Figure A4-3a and the data is presented in Table A4-3 below.*

Table A4-3. SEM-EPMA point analyses of the bentonite in contact with carbon steel coupon at 30°C. The location of point analyses are marked in Figure A4-3a.

No.	Na	Mg	Al	Si	S	Cl	K	Ca	Mn	Fe	O
45	2.11	1.75	9.76	27.58	0.01	0.23	0.10	0.77	0.01	7.20	50.48
47	1.84	1.45	9.78	27.81	0.02	0.33	0.09	0.86	0.00	5.08	52.74
49	1.31	1.42	9.48	29.92	0.02	0.32	0.22	0.62	0.00	3.03	53.68
51	1.71	1.38	9.91	29.11	0.01	0.32	0.15	1.42	0.00	3.29	52.71
53	1.58	1.43	9.77	30.94	0.07	0.43	0.22	0.98	0.00	2.79	51.79
55	1.81	1.74	11.74	26.92	0.00	0.32	0.11	0.68	0.00	3.33	53.34
57	3.07	1.14	11.97	25.83	0.01	0.28	0.42	0.99	0.00	2.23	54.04
59	1.87	1.29	10.66	24.32	0.01	0.30	0.28	0.64	0.01	3.22	57.41
61	0.75	0.24	1.71	3.05	1.77	0.21	0.04	0.45	0.00	0.92	90.85
63	0.47	0.43	4.25	39.05	0.02	0.30	1.12	0.21	0.01	1.31	52.83
65	1.87	1.69	9.25	19.85	0.10	0.35	0.21	3.31	0.02	2.49	60.86
67	1.82	1.56	10.98	27.98	0.02	0.27	0.11	0.52	0.00	2.88	53.86
69	1.43	1.30	9.04	31.97	0.04	0.38	0.10	0.56	0.01	2.35	52.83
71	1.72	1.53	12.81	28.04	0.01	0.28	0.12	0.34	0.00	2.59	52.57
73	1.74	1.59	13.09	28.37	0.01	0.27	0.12	0.38	0.00	2.52	51.91
75	1.72	1.39	11.32	24.96	0.01	0.30	0.11	0.38	0.00	2.22	57.60
77	1.77	1.47	10.34	29.14	0.17	0.46	0.08	0.69	0.00	2.18	53.69
79	1.23	1.34	9.81	24.16	0.02	0.51	0.14	0.50	0.00	2.14	60.15
81	0.97	0.85	6.02	13.07	0.00	0.24	0.05	0.22	0.01	1.12	77.44
83	1.85	1.69	12.68	28.82	0.02	0.33	0.11	0.43	0.00	2.47	51.61
85	0.82	0.91	8.26	33.82	0.01	0.50	1.41	0.68	0.00	1.61	51.97
87	1.64	1.57	11.91	26.09	0.01	0.32	0.08	1.06	0.00	2.52	54.80

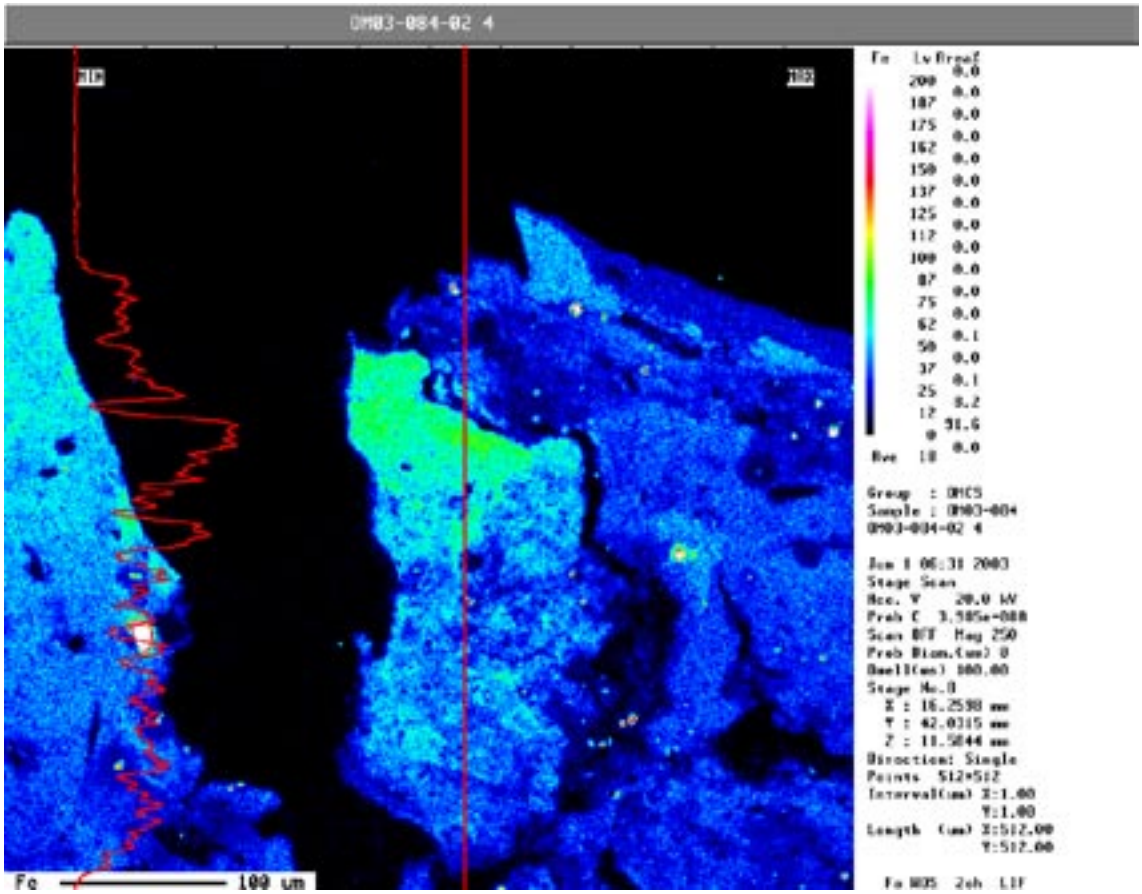

Figure A4-4. *Iron image of compacted bentonite in contact with a cast iron coupon for 256 days at 50°C. The contrast on the iron intensity has been increased. Vertical line shows the position of the iron profile (left of image).*

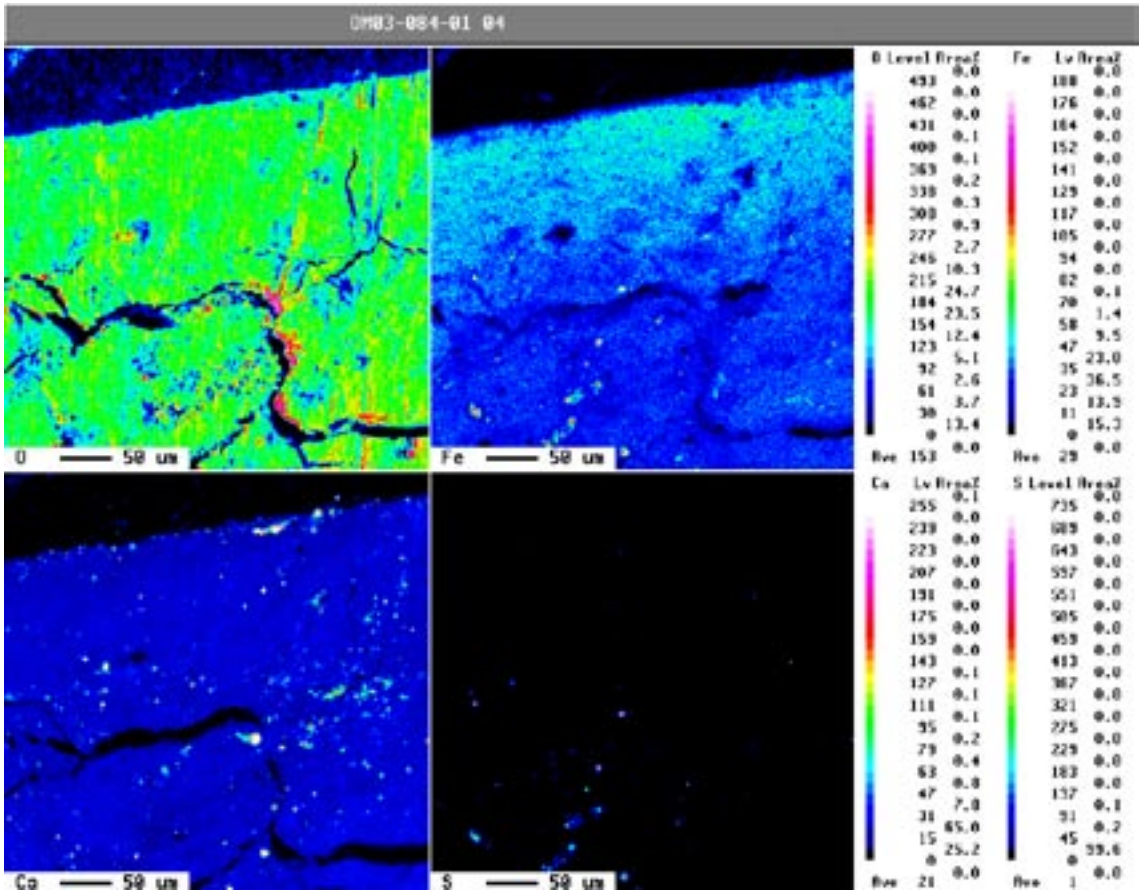

Figure A4-5. *EPMA mapping of compacted bentonite in contact with a carbon steel coupon for 356 days at 50°C.*